AGU PUBLICATIONS

Tectonics

RESEARCH ARTICLE
10.1002/2017TC004766

Key Points:
- We identify and bracket the timing of Plio-Quaternary thrust inversion of Miocene extensional faults in the eastern Tohoku fore arc
- Faults have listric geometries with 40–65° west dipping ramps that sole to subhorizontal detachments at 6–10 km depth
- These faults may experience slip inversion in response to changes in stress state over time scales ranging from 10^1 to 10^6 years

Supporting Information:
- Supporting Information S1

Correspondence to:
C. Regalla,
cregalla@bu.edu

Citation:
Regalla, C., Fisher, D. M., Kirby, E., Oakley, D., & Taylor, S. (2017). Slip inversion along inner fore-arc faults, eastern Tohoku, Japan. *Tectonics*, *36*, 2647–2668. https://doi.org/10.1002/2017TC004766

Received 14 AUG 2017
Accepted 21 OCT 2017
Accepted article online 4 NOV 2017
Published online 24 NOV 2017

Slip Inversion Along Inner Fore-Arc Faults, Eastern Tohoku, Japan

Christine Regalla[1], Donald M. Fisher[2], Eric Kirby[3], David Oakley[2], and Stephanie Taylor[4]

[1]Department of Earth and Environment, Boston University, Boston, MA, USA, [2]Department of Geosciences, Penn State University, University Park, PA, USA, [3]College of Earth, Ocean, and Atmospheric Sciences, Oregon State University, Corvallis, OR, USA, [4]Department of Earth and Planetary Sciences, University of California, Santa Cruz, CA, USA

Abstract The kinematics of deformation in the overriding plate of convergent margins may vary across timescales ranging from a single seismic cycle to many millions of years. In Northeast Japan, a network of active faults has accommodated contraction across the arc since the Pliocene, but several faults located along the inner fore arc experienced extensional aftershocks following the 2011 Tohoku-oki earthquake, opposite that predicted from the geologic record. This observation suggests that fore-arc faults may be favorable for stress triggering and slip inversion, but the geometry and deformation history of these fault systems are poorly constrained. Here we document the Neogene kinematics and subsurface geometry of three prominent fore-arc faults in Tohoku, Japan. Geologic mapping and dating of growth strata provide evidence for a 5.6–2.2 Ma initiation of Plio-Quaternary contraction along the Oritsume, Noheji, and Futaba Faults and an earlier phase of Miocene extension from 25 to 15 Ma along the Oritsume and Futaba Faults associated with the opening of the Sea of Japan. Kinematic modeling indicates that these faults have listric geometries, with ramps that dip ~40–65°W and sole into subhorizontal detachments at 6–10 km depth. These fault systems can experience both normal and thrust sense slip if they are mechanically weak relative to the surrounding crust. We suggest that the inversion history of Northeast Japan primed the fore arc with a network of weak faults mechanically and geometrically favorable for slip inversion over geologic timescales and in response to secular variations in stress state associated with the megathrust seismic cycle.

1. Introduction

The fore-arc regions of subduction zones, like that of Northeast Honshu, Japan, are constructed and deformed over multiphase histories and evolve in response to changes in the subducting bathymetry (e.g., Audin et al., 2008; Bangs et al., 2006; Fisher et al., 1998; Gardner et al., 2001; Hampel, 2002; Kington & Tobin, 2011; Morell et al., 2011; Regard et al., 2009; Wang & Bilek, 2011), convergence rate and obliquity (e.g., Allmendinger & González, 2010; Morell, 2016; Regalla, Fisher, et al., 2013), mechanical properties of the megathrust (e.g., Allmendinger & González, 2010; Buiterr et al., 2001; Hassani et al., 1997; Saffer & Tobin, 2011), and variations in slab geometry (e.g., Capitanio et al., 2009; Capitanio et al., 2010; Royden & Husson, 2006). Variations in stress state during such deformation events can lead to the development of networks of upper plate faults that can act as structural weaknesses available to be reactivated in response to subsequent changes in boundary conditions at the plate interface. The low shear strength documented on subduction interfaces, indicated by direct and indirect observations and modeling (e.g., Allmann & Shearer, 2009; Fisher & Byrne, 1987; Fulton et al., 2013; Hasegawa et al., 2011; Tobin & Saffer, 2009; Ujiie & Kimura, 2014; Wang et al., 1995) and by low magnitudes of fore-arc differential stress determined from focal mechanism inversions (Balfour et al., 2011; Wang et al., 1995; Yang et al., 2013; Yoshida et al., 2015), implies that the fore arc is structurally weak, a state that could be maintained by deformation along networks of upper plate faults with low shear strength or high fluid pressures. Such faults may be able to fail in response to relatively small changes in stress field (e.g., Loveless et al., 2010; Sibson, 2009) and may have temporally variable kinematics that evolve in response to changes in stress state related to variation in plate boundary dynamics and kinematics over both geologic (10^6 yr) timescales (e.g., Hassani et al., 1997; Heuret et al., 2007; Heuret & Lallemand, 2005; Lallemand, Heuret, & Boutelier, 2005; Lallemand et al., 2008) and in response to the loading and unloading of the upper plate during the seismic cycle (e.g., Farías et al., 2011; Hasegawa et al., 2011; Loveless et al., 2010; Ryder et al., 2012; Sherrod & Gomberg, 2014; Toda, Lin, & Stein, 2011; Toda, Stein, & Lin, 2011). The kinematics of deformation along these faults therefore need not be temporally constant, and their deformation history contains a record of past variations in upper plate stress state in response to changes in tectonic forcing at the plate boundary.

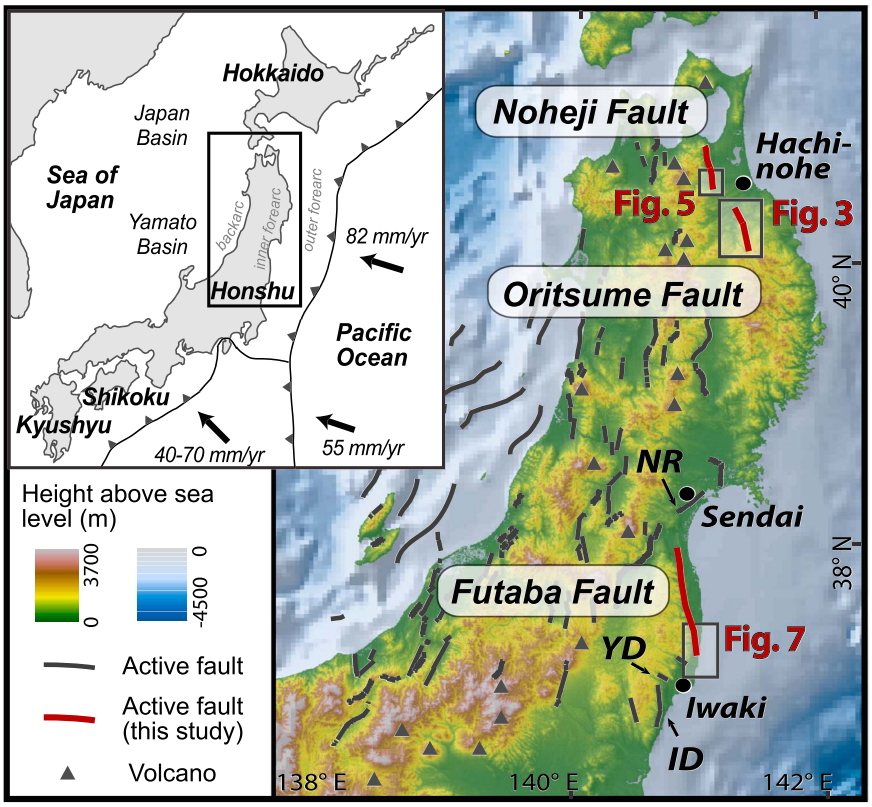

Figure 1. Digital elevation and bathymetry of northern Honshu showing the surface traces of active faults (National Institute of Advanced Industrial Science and Technology, 2012), the location of the Oritsume, Noheji, and Futaba Faults, and active volcanoes. ID: Idosawa Fault, YD: Yunodake Fault, NR: Nagamachi-Rifu Fault. Elevation and bathymetry from SRTM3 and ETOPO2 data sets, respectively. Inset shows regional geologic setting.

The Tohoku margin of northern Japan is an example of a subduction fore arc that contains a network of inherited faults that have accommodated permanent strain in response to changes in stress state over the Jurassic to present (Ikeda et al., 2002; Jolivet, Tamaki, & Fournier, 1994; Okada & Ikeda, 2012; Regalla, Fisher, et al., 2013; Sato & Amano, 1991) (Figure 1). Today, active E-W directed upper plate contraction occurs over a >500 km wide region inboard of the Japan trench, across both the fore arc and the back arc (e.g., Ikeda et al., 2002; Okamura, 2003; Regalla et al., 2010; Sato et al., 2002; Wesnousky et al., 1984). Contractional deformation in the back arc is attributed to Plio-Quaternary thrust inversion of listric, extensional faults originally formed during Miocene opening of the Sea of Japan (Okada & Ikeda, 2012; Okamura et al., 1995; Sato & Amano, 1991), but comparatively less is known about the geometry, kinematics, and timing of deformation along faults in the inner fore arc. Interestingly, several recent *M*6+ upper plate fore-arc aftershocks that occurred following the 2011 *M*9 Tohoku-oki megathrust earthquake had normal displacement consistent with ~E-W directed extension (e.g., Hasegawa et al., 2012; Hirose et al., 2011; Imanishi et al., 2012; Kato et al., 2011; Kobayashi et al., 2012; Okada et al., 2011), opposite the sense of long-term E-W directed contraction documented across the arc. These observations indicate the potential for reversals in slip along fore-arc faults not only over geologic time scales but also in response to static stress changes or viscoelastic transients following megathrust events (Miyazawa, 2011; Sun et al., 2014; Toda, Lin, & Stein, 2011; Wang et al., 2012). Such reversals in slip appear to require the presence of weak faults that can fail in response to small changes in the magnitude and orientation of the stress field. These aftershocks occurred onshore in populated areas (e.g., Imanishi et al., 2012; Okada et al., 2011) and highlight the need to understand the geometry and kinematics of fore-arc faults in order to assess how these faults respond to variations in stress state during the loading and unloading of the upper plate during the seismic cycle.

Here we document the Neogene kinematic history and subsurface geometry of faults in the fore arc of Northeast Honshu, Japan, in order to identify structural and stratigraphic evidence for tectonic inversion, to bracket the timing of deformation, and to quantify the geometry of faults potentially susceptible to

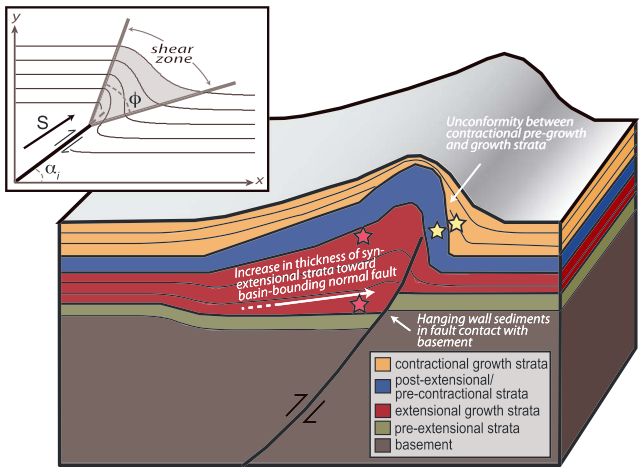

Figure 2. Schematic block diagram showing idealized cross section of an inverted listric fault with synextensional and syncontractional growth strata. Extensional growth strata thicken toward the fault and have a total hanging wall thickness greater than the footwall. Syncontractional strata thin above the fault-related fold and onlap older tilted strata. The red stars denote the location of dated strata at the base and top of extensional growth strata that bracket the duration of normal faulting. The yellow stars denote dated strata in contractional pregrowth and growth strata that bracket the onset of thrusting. Inset shows parameters used in trishear modeling. The shape of a fault-related fold is dictated by local fault dip (α_i), total fault slip (S), the angular width of the shear zone (φ), fault with a position in x-y space, and the ratio of fault tip propagation to fault slip.

inversion. We focus on three prominent active structures: the Oritsume, Noheji, and Futaba Faults. These faults are active, west dipping, contractional structures that bound basement-involved structural massifs in the inner fore arc of Northeast Japan. All three structures are candidates for Plio-Quaternary thrust inversion of Miocene extensional structures as they are located ~50–75 km east of faults with well-documented inversion histories (e.g., Nakajima, 2006; Okada & Ikeda, 2012; Okamura, 2003). In addition, these structures are located within the region that experienced an increased rate of upper plate seismicity following the 2011 Tohoku-oki earthquake (Hasegawa et al., 2012; Toda, Lin, & Stein, 2011; Toda, Stein, & Lin, 2011) and are candidate faults that could experience slip in response to changes in stress field following megathrust rupture events. Our data indicate a history of thrust inversion of inherited normal faults in the fore arc of Northeast Japan, along structures which may have geometries and mechanics that make them candidates for failure in response to both long-term geologic forcing and short-term variations in stress state during the subduction seismic cycle.

2. Geologic Setting

The northern part of Honshu Island is situated at the convergent boundary where the Pacific plate subducts beneath Eurasia at a rate of ~82 mm/yr (Niitsuma, 2004; Seno et al., 1993) (Figure 1). Subduction along the western Pacific margin since at least the Jurassic (Isozaki, 1997; Isozaki et al., 1990) has resulted in the accretion of Jurassic to Cretaceous rocks and emplacement of Cretaceous granitoids (Hiroi et al., 1998; Iwata et al., 2000; Kimura, 1994; Saito & Hashimoto, 1982) that comprise the basement across much of Northeast Japan. The upper plate along this convergent margin experienced early to middle Miocene back-arc extension (25–15 Ma) and extrusion of seafloor basalts (24–18 Ma) associated with the rifting of the eastern Asian margin and the formation of the Sea of Japan (Jolivet & Tamaki, 1992; Kaneoka et al., 1990). Miocene rift-related half-grabens that extend across western Honshu are recognized in the back arc and volcanic arc (Kato et al., 2006; Sato et al., 2002; Sato & Amano, 1991). Northeast Japan transitioned to an arc-normal compressional stress regime during the late Miocene to early Pliocene (Sato, 1994), and late Neogene shortening has been documented along a network of reverse faults and fault-related folds (e.g., Okada & Ikeda, 2012; Sato & Amano, 1991; van der Werff, 2000), many of which resulted from thrust inversion of inherited extensional structures. In this study, we investigate the potential inversion histories of three prominent faults in the inner fore arc of Northeast Japan, the Oritsume, Noheji, and Futaba Faults (Figure 1). Below we briefly describe the local stratigraphy used to reconstruct subsurface fault geometry and in which we identify extensional and contractional growth sequences (Figure 2).

The Oritsume Fault is an ~30 km long, N-S striking, west dipping thrust fault located ~20 km west of the town of Hachinohe (Figures 1 and 3a). Here basement rocks consisting of Jurassic and Cretaceous accreted subduction complexes are overlain by a series of early Miocene to Pliocene siliciclastic and volcaniclastic deposits (Figure 4). The basal Miocene Yotsuyaku Formation contains lignite-bearing terrestrial sediments and

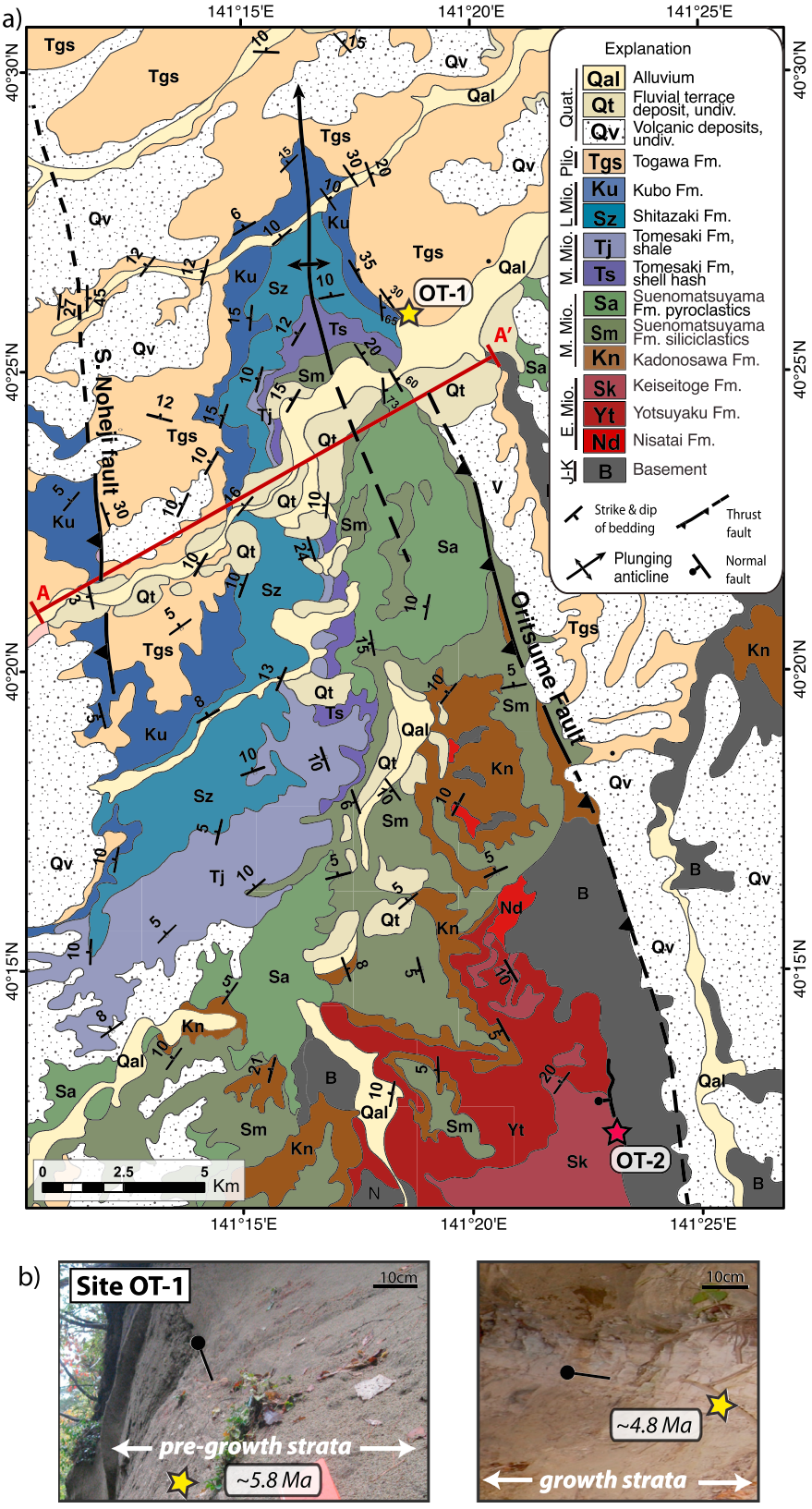

Figure 3. (a) Geologic map of the area surrounding the Oritsume Fault after Kamada et al. (1990), showing line of section A-A′, in Figure 9. See Figure 1 for location and Figure 4 for stratigraphy. (b) Field photo of the unconformity separating contractional pregrowth (dip of ~50°E) and growth (dip of <10°E) strata at site OT-1. U-Pb zircon ages from tephras sampled at approximate location of stars.

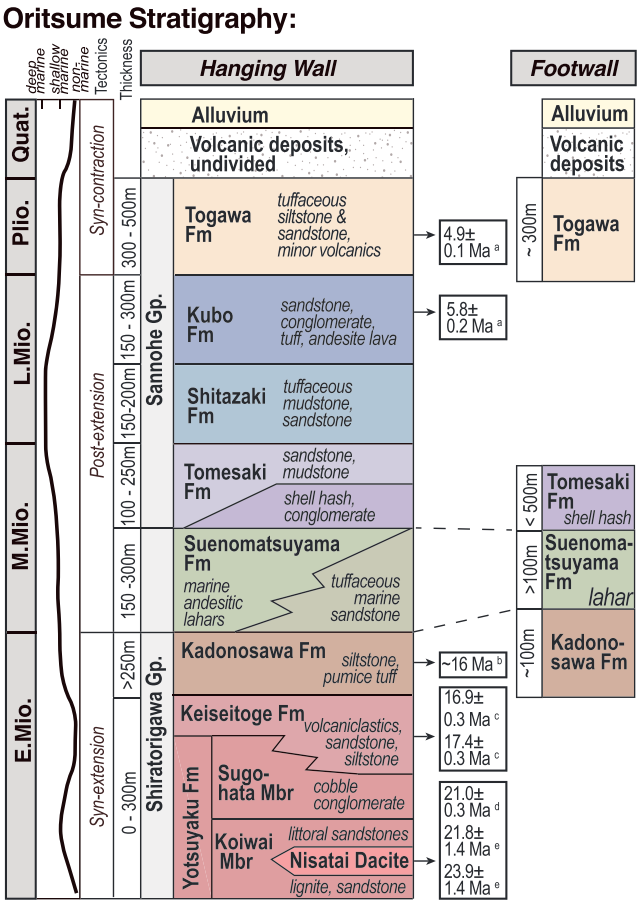

Figure 4. Stratigraphy of the region surrounding the Oritsumerjrault (after Chinzei, 1966; Kamada et al., 1990; Yagishita & Komori, 2000). (a) U-Pb zircon, *this study*; (b) Foram Zone N8 (Irizuki & Matsubara, 1994); (c) K-Ar (Ishizuka & Uto, 1995); (d) K-Ar (Tagami et al., 1995); and (e) Fission track (Tagami et al., 1995).

transitions up section to shallow marine siliciclastics interbedded with the volcaniclastic Keiseitoge Formation (Yagishita & Komori, 2000). Overlying these are the marine siliciclastic units of the Kadonosawa and Suenomatsuyama Formations, pyroxene andesite lahars of the Suenomatsuyama Formation, and marine sediments and volcanics of the Tomesaki, Shitazaki, Kubo, and Togawa Formations (Chinzei, 1966; Kamada et al., 1990). This stratigraphic section has been folded into a north plunging fault-related anticline developed in the hanging wall of the Oritsume Fault. All units are present in the hanging wall, but only the Kadonosawa, Suenomatsuyama, Tomesaki, and Togawa Formations are present in the footwall of the fault (Figures 3a and 4).

The Noheji Fault, also mapped as the Muriyama Fault, is a N-S striking, west dipping fault with a discontinuous surface expression for ~20 km length, located ~ 25 km northwest of the Oritsume Fault (Figures 1 and 5a). The oldest exposed units in the hanging wall of the Noheji Fault are early Neogene volcanic rocks and tuffaceous sandstones (Ozawa & Mimura, 1993; Tsushima, 1962). These units are overlain by diatomaceous siltstones and sandstones of the Wadagawa Formation (Yamaguchi, 1970), locally also mapped as the Gamanosawa and Shitazaki Formations (Tsushima, 1962), which interfingers with the andesitic lahars and tuff-breccias of the Tomari Formation (Figure 6). The youngest units in the region are the shallow marine siliciclastics of the Togawa Formation, locally mapped as the Sunagomata Formation, and Quaternary volcanic deposits, marine terrace deposits, and volcanic ash. These Miocene through Pliocene units are folded into a hanging wall anticline that extends for ~40 km (Figure 5a).

The Futaba Fault system is a N-S striking, ~100 km long west dipping thrust fault located north of the town of Iwaki, ~350 km south of the Oritsume and Noheji faults (Figure 7). In this region, Cretaceous granitic basement is overlain by sequences of Cretaceous to Pliocene sedimentary units (Figure 8). The basal Cretaceous and Paleogene coal-bearing Futaba and Shiramizu groups (Kubo et al., 2003; Mitsui, 1971) are unconformably overlain by fluvial, shallow marine, and deep marine siliciclastics of the Miocene Yunagaya, Shirado, and Takaku groups and shallow marine sandstones and mudstones of the Taga and Sendai groups (Kubo et al., 2002; Suto et al., 2005). This sedimentary sequence is deformed into an ~100 km long fault-related fold, and only units of the Shiramizu, basal Yunagaya, Taga, and Dainenji groups are present in the footwall of the fault (Figures 7 and 8).

3. Approach and Methods

We used a combination of field mapping, dating of growth strata, and kinematic fault-related fold modeling to document the geometry and structural history of the Oritsume, Noheji, and Futaba Faults.

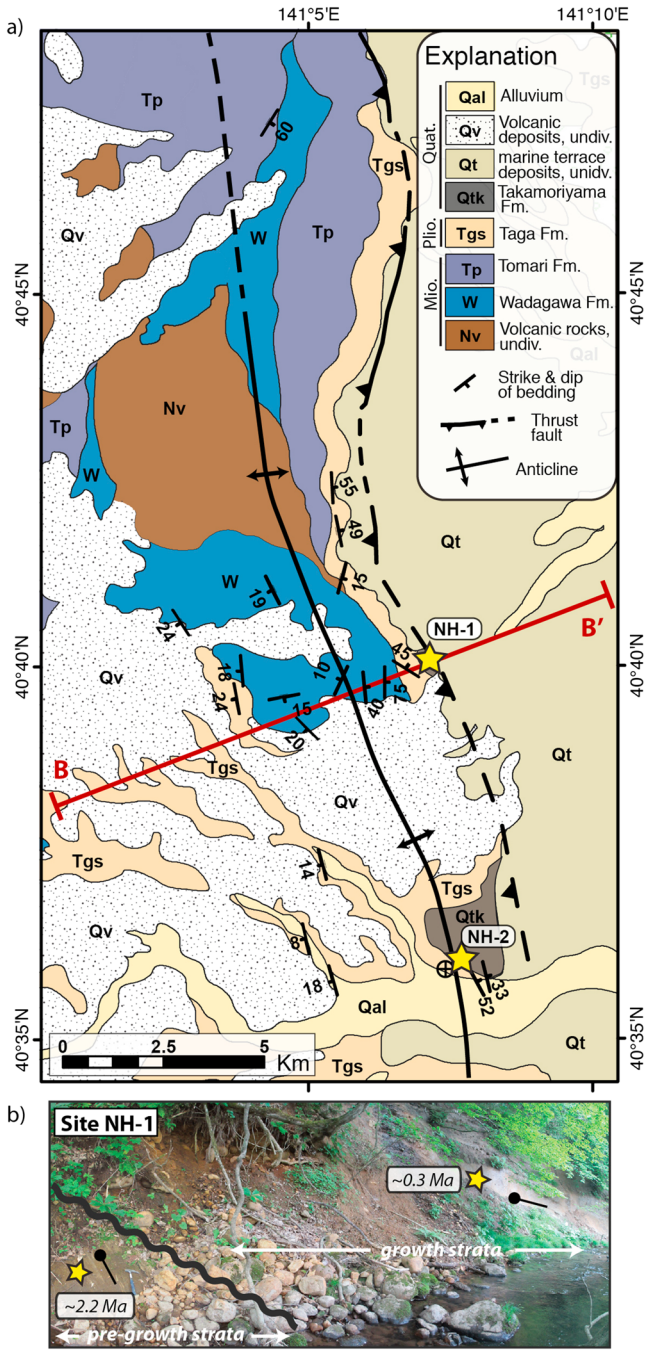

Figure 5. (a) Geologic map of the area around the southern portion of the Noheji Fault (after Tsushima, 1962; Kudo, 2005). Map shows line of section B-B′ in Figure 10, and locations of identified growth and pregrowth strata (sites NH-1 and NH-2). See Figure 1 for location and Figure 6 for stratigraphy. (b) Field photo of the unconformity separating contractional pregrowth (dip of ~46°E) and growth (dip of ~10°E) strata at site NH-1. U-Pb zircon ages from tephras sampled at approximate location of stars.

First, we combined new field structural mapping with published geologic maps and stratigraphic sections (Kamada et al., 1990; Kubo et al., 2002; Kudo, 2005; Tsushima, 1962) to document structural and stratigraphic evidence for Plio-Quaternary contractional inversion of preexisting Miocene extensional faults. Second, we identified growth strata associated with extensional and contractional deformation and bracket the timing and duration of deformation by combining four new U-Pb dates with existing geochronology and biostratigraphy in the growth sequences (Chinzei, 1966; Regalla et al., 2010; Regalla, Kirby, et al., 2013; Yagishita & Komori, 2000). Third, we used forward and inverse trishear kinematic modeling of contractional fault-related fold geometry to determine the subsurface geometry of each fault, to test if slip along the same fault geometry can reproduce both extensional and contractional deformation.

3.1. Identification and Dating of Growth Strata

We utilized field structural mapping and dating of newly identified growth strata to determine the Neogene deformation history of the Oritsume, Noheji, and Futaba Faults in the inner fore arc of Northeast Japan. New field data were integrated with published 1:200,000 and 1:50,000 scale geologic maps (Kamada et al., 1990; Kubo et al., 2002; Kudo, 2005; Tsushima, 1962) and existing structural data and stratigraphy (Chinzei, 1966; Regalla et al., 2010; Regalla, Kirby, et al., 2013; Yagishita & Komori, 2000) to quantify fault-related fold geometry and thicknesses of syndeformational growth strata. Growth strata deposited during contraction occur on the limbs of fault-propagation folds developed in association with active thrust faults. A progressive unconformity may occur in the stratigraphy separating pregrowth strata with steep dips from growth strata whose dips decrease up-section (e.g., Buchanan & McClay, 1991; Mitra & Islam, 1994). Growth strata associated with extension occur in the hanging walls of normal faults. These sequences often display an increase in total thickness toward the fault and a divergence in bedding dip between the base and top of the growth sequence (e.g., Buchanan & McClay, 1991; Mitra & Islam, 1994).

The timing of extensional and contractional deformation was determined from geochronologic and biostratigraphic ages of newly identified growth strata. The onset of contractional deformation was determined from four new U-Pb dates in zircons and from existing tephrachronology (Kudo, 2005; Suto et al., 2005) in ashes collected from above and below unconformities that separate the pregrowth and growth sections in the forelimbs of contractional fault-related folds (Figure 2, yellow stars). New tephra ages were determined by laser ablation U-Pb zircon geochronology at the Laser-Ablation Split Stream Petrochronology Lab, University of California, Santa Barbara (Kylander-Clark et al., 2013), where for each sample, 40–50 measurements were obtained, and $^{206}Pb/^{238}U$ ages and errors were modeled using the TuffZirc algorithm (Ludwig & Mundil, 2002). The timing of extension is bracketed by published $^{39}Ar/^{40}Ar$, zircon fission track, and biostratigraphic ages from the base and top of synextensional stratigraphic sections (Figure 2, red stars).

3.2. Fault Geometry and Slip From Kinematic Modeling

We used trishear kinematic modeling to determine the subsurface fault dip and geometry of inner fore-arc faults and test whether observed structural and stratigraphic data can be reproduced through contractional inversion of extensional faults. Fault geometry and total slip were constrained using trishear kinematic

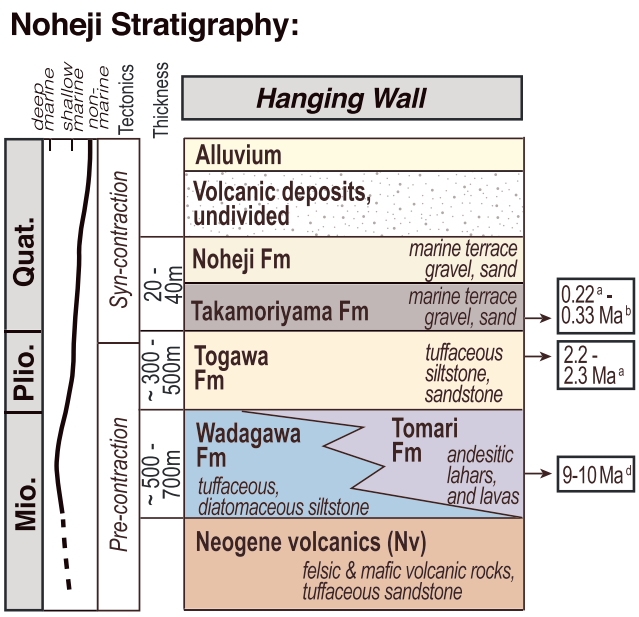

Figure 6. Stratigraphy of the region surrounding the Noheji Fault (after Aoyagi & Omokawa, 1993; Kamada et al., 1990; Tsushima, 1962). (a) U-Pb zircon, *this study*; (b) Bo-P tephra (Machida et al., 1985; Miyauchi, 1988); (c) K-Ar (Kudo, 2005); and (d) Diatom Zone N14-N15 (Aoyagi & Omokawa, 1993).

forward modeling, performed using Midland Valley's 2D Move™ software package, and inverse trishear kinematic modeling using the methods of Oakley and Fisher (2015). The trishear kinematic model has been used as an alternative to kink band fold kinematics to explain the downward tightening and convergence of fold hinges and changes in stratigraphic thickness and limb dip observed in basement-involved, fault-related folds (Allmendinger, 1998; Erslev, 1991). This kinematic model produces simple shear within a triangular zone fixed to a propagating fault tip (Figure 2, inset) (Allmendinger, 1998; Erslev, 1991). Bedding is deformed such that the divergence of the velocity field within the shear zone is zero and results in area-balanced cross sections.

The shape of the fault-propagation fold in a trishear model is a function of the shear zone geometry and the rate and direction of shear zone propagation through the overlying strata (Allmendinger, 1998), assuming fold formation results from mass transfer within the plane of section. The geometry of the fold is defined by the following kinematic model parameters: (1) fault dip (α_i), which can vary in space for nonplanar fault geometries; (2) the position of the fault tip at the initiation of deformation in *x-y* space; (3) total displacement (*S*); (4) the ratio of fault tip propagation (*P*) to fault slip (*P/S* ratio); and (5) the angular width of the shear zone (ϕ) (Figure 2, inset).

Forward modeling was conducted iteratively in three stages. First, initial constraints on allowable fault geometries were determined by forward kinematic modeling in 2D Move (Midland Valley Exploration Ltd.) to replicate the contractional fault-related fold geometry within the post extensional sediment sequence along the Oritsume, Noheji, and Futaba Faults, assuming fold formation via dip slip. These models were used to determine the range of fault geometry (α_i, as a function of cross-sectional distance) and total dip slip (*S*) that best replicate the position and dip of bedding contacts projected onto cross lines of cross section, given variable fault tip position, ϕ, and *P/S* ratios (Table 1). For the Futaba Fault, fault geometry was constrained by published results of Monte Carlo simulations of fault dip and modeling of the evolution of hanging wall fluvial profiles in response to active uplift (Regalla et al., 2010; Regalla, Kirby, et al., 2013). In order to determine the robustness of the modeled fault geometries and assess uncertainty in ramp dip and detachment depth, fault-related fold geometry was independently modeled following the inverse method of Oakley and Fisher (2015). This method restores bedding dips and locations of contacts along a cross section in order to invert for fault geometry and trishear parameters using a Markov chain Monte Carlo approach. The inverse models solve for the deformation field using the listric fault trishear kinematics of Cardozo and Brandenburg (2014) assuming inclined shear in the hanging wall, and a fault geometry that includes a planar, subhorizontal detachment and planar, high-angle ramp connected by a fault segment prescribed as a circular arc segment.

Second, for faults where Miocene extensional growth strata were identified, fault geometries determined in the first step were used to model extensional displacement of initially flat lying strata, assuming deformation via dip slip. Total extension was initially approximated by the difference in sediment thickness between the hanging wall and footwall of modeled structures. Best fit total extension was determined through iterative modeling of the extensional structure, given the best fit fault geometry determined as above, and published stratigraphic thicknesses (Chinzei, 1966; Kamada et al., 1990; Kudo, 2005; Suto et al., 2005). Fault tip position, ϕ, and *P/S* ratios were varied in order to produce reasonable sediment distributions and to provide suitable starting conditions for modeling of thrust inversion (Table 1).

Third, using postextension cross-sectional geometries as determined above, faults were subjected to contractional inversion, given the ranges of *S*, ϕ, and *P/S* determined initially. Iterative repetitions of extension and thrust inversion were modeled until a set of parameters converged that best reproduced observed stratal thickness variations, bed dips, and fold geometries for both the extensional and contractional stages of deformation. For all stages of modeling, goodness of fit was determined by inspection of final deformed-state cross sections. Sections were rejected if model and observed bedding dips differed by more than ~10° or if model and

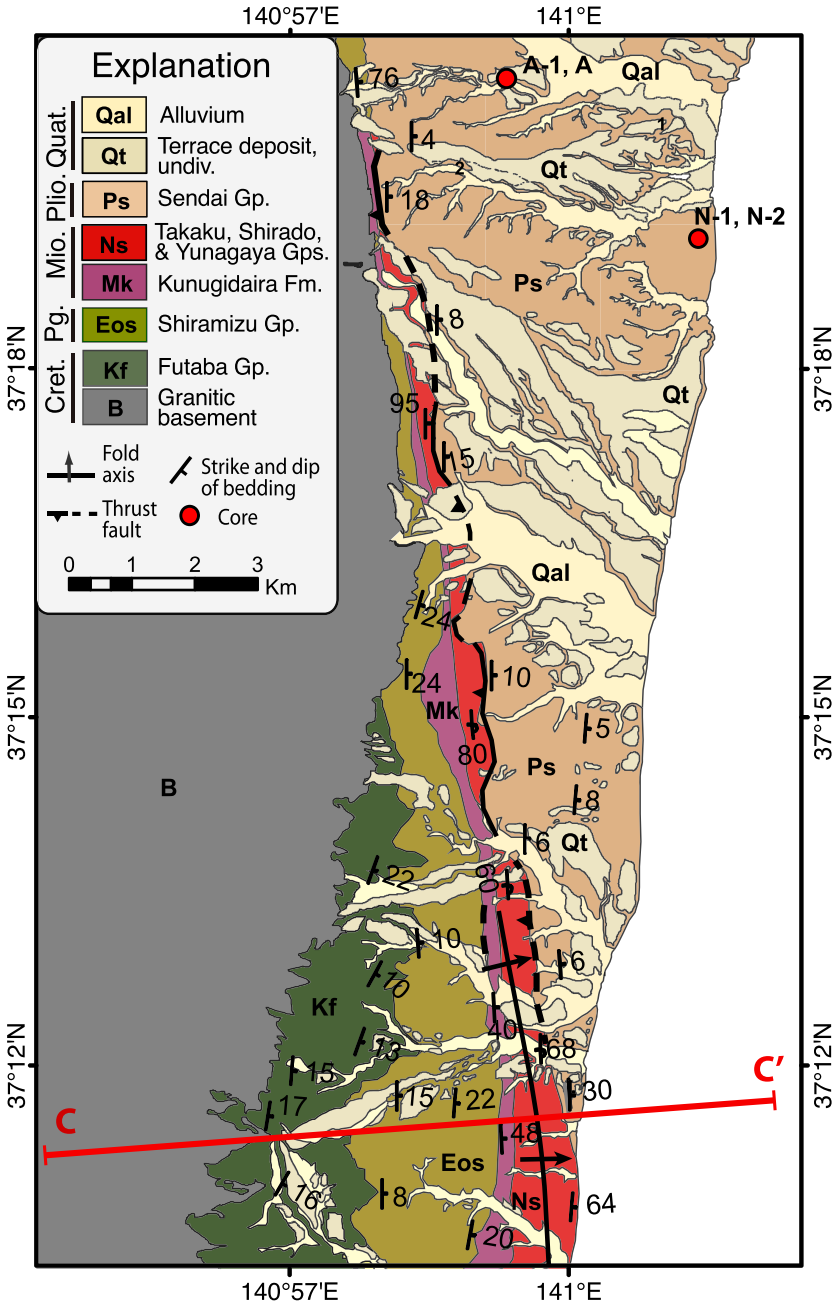

Figure 7. Geologic map of the southern tip of the Futaba Fault (after *Geological Survey of Japan*, *AIST*, 2003; Kubo et al., 2002). Map shows line of section C-C′ in Figure 11, and locations of cores that constrain sediment thickness in the footwall. See Figure 1 for location and Figure 8 for stratigraphy.

observed contact positions differed by more than ~100 m. Best fit fault geometries were then used to estimate the range of stress conditions under which slip inversion could occur in the fore arc of Northeast Japan.

4. Results

Below we discuss evidence for Plio-Quaternary contraction and Miocene extension along the Oritsume, Noheji, and Futaba Faults, and the geometries of structures that accommodate slip inversion. First, we discuss thrust fault-related fold geometries and present evidence for the timing of initiation of contraction through dating of growth strata. Second, we present evidence for Miocene extension and tectonic inversion along inherited structures in the inner fore arc. Third, we use structural and stratigraphic data from thrust fault-

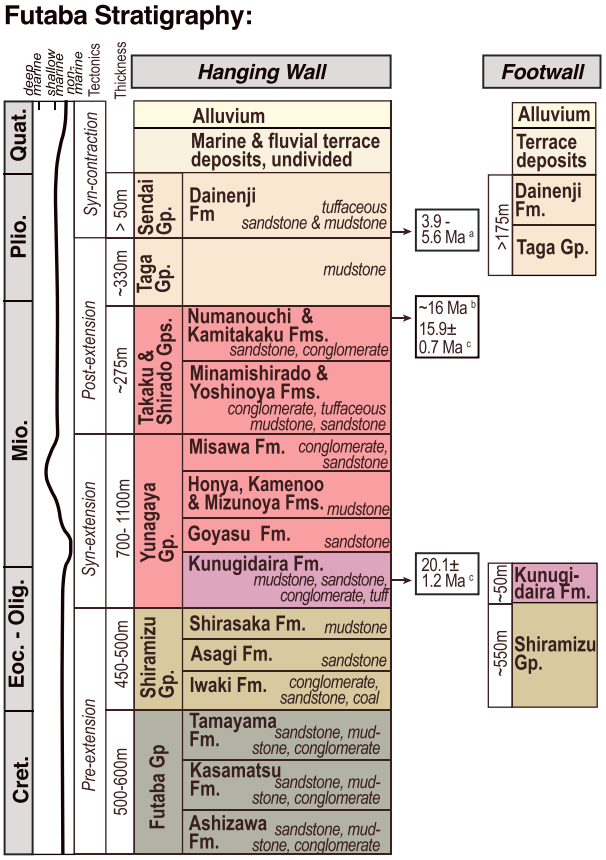

Figure 8. Stratigraphy of the region surrounding the Futaba Fault (after Kubo et al., 2002; Suto et al., 2005). (a) Zircon fission track in tephra (Suto et al., 2005); (b) diatom, (Suto et al., 2005); and (c) fission track (Suto et al., 2005).

related folds as inputs in trishear kinematic models to quantify subsurface fault dip and to model the extensional and contractional inversion history of fore-arc structures. Finally, we use these results to place bounds on the total magnitudes of normal and thrust displacement and to evaluate the geometry and mechanics of faults susceptible to slip inversion in the fore arc of Northeast Japan.

4.1. Plio-Quaternary Contraction

Fault-related folds developed in the Mio-Pliocene sedimentary sequence at the northern and southern tips of the Oritsume, Noheji, and Futaba Faults indicate a component of reverse separation along each structure during the Neogene (Kamada et al., 1990; Kubo et al., 2002; Tsushima, 1962). Growth strata associated with the formation of these folds have the following characteristics (Figure 2): (1) Growth strata are preserved on the forelimb of folds, near the lateral fault tip where the thrust fault transitions from emergent to blind. (2) The steep dips of pregrowth strata transition up section to gentle or subhorizontal dips over a strike-orthogonal distance on the order of 50–75 m. (3) There may be a progressive unconformity separating pregrowth and growth strata that becomes conformable toward the lateral fault tip. (4) The thicknesses of growth sequences are greatest in the footwall of thrust, and thin toward the hanging wall. Below we discuss the stratigraphy, fold geometry, and growth strata identified along the Oritsume and Noheji fore-arc faults and present new evidence for the timing of contraction along these structures. Thrust fault-related fold geometry and ages of growth strata along the Futaba Fault have been previously published (Regalla et al., 2010) and are therefore not discussed here.

4.1.1. Oritsume Fault

We identifed and mapped contractional growth strata within the Togawa Formation in the forelimb of the Oritsume fault-related fold that bracket the timing of Plio-Quaternary shortening along the Oritsume Fault (Figure 3a, site OT-1). Steeply dipping (strike and dip of 350°, 50°E) rocks of the upper Kubo Formation in the forelimb of the anticline are overlain by gently east dipping (strike and dip of 380°, 20°E) beds of the Togawa Formation (Figure 3b). Outcrops ~50–70 m stratigraphically above the gently dipping Togawa beds display subhorizontal bedding (Figure 3b). In contrast, in outcrops along strike ~2 km north of this location in the forelimb of the fault-related fold, beds of the Kubo and Togawa Formations do not show a variation in dip up section but have comparable, gentle (10–20°) dips. These up-section decreases in bedding dip are best explained as growth strata deposited during the formation of the fault-related fold.

We determined two new U-Pb zircon ages from tephras interbedded with pregrowth and growth strata (Figure 3b) to bracket the timing of initiation of contraction along the Oritsume Fault. A tephra from the steeply dipping pregrowth beds of the Kubo Formation yielded an age of 5.78 (+0.19, −0.05) Ma, and a tephra from the gently dipping growth beds of the Togawa Formation yielded an age of 4.87 (+0.06, −0.08) Ma

Table 1
Parameter Space and Best Fit Values for Trishear Kinematic Models

	Fault angle	Detachment depth	Extension: Slip	Extension: P:S/ϕ	Contraction: Slip	Contraction: P:S/ϕ
Oritsume Fault						
Parameter space	40°–80°	6–10 km	300–1500 m	1–2/30°–90°	500–2000 m	0.5–2.6/30°–90°
Best fit forward models	55°–65°	6–7 km	400–750 m	1.7–2/40°–60°	1800–2000 m	1.5–2/60°–70°
Best fit inverse models[a]	46°–57°	6–7.5 km	–	–	1440–1960 m	1.3–1.7/38–76
Noheji Fault						
Parameter space	45°–65°	6–7 km	–	–	100–1500 m	1.0–3.0/40°–80°
Best fit forward models	55°–65°	6 km	–	–	860–1100 m	2.4–2.8/40°–60°
Best fit inverse models[a]	46°–64°	6–7 km	–	–	660–1160 m	>1.3 / 20°–52°
Futaba Fault						
Parameter space	38°–62°[b,c]	10 km [b,c]	500–2000 m	0.6–2.2/20°–90°	1600–3600 m [c]	0.6–2.2/49°–115° [c]
Best fit forward models	40°–55°	10 km	1000–1500 m	1–1.5/30°–60°	2300–2800 m [c]	1.7–2.1/80°–110° [c]
Best fit inverse models[a]	39°–58°	-----	–	–	2120–2720 m	1.8–2.2/87°–98°

[a]Results reported given 95% confidence intervals. [b]Fault geometry following Regalla, Kirby, et al. (2013). [c]Model parameters following Regalla et al. (2010).

(Figure 3b). These samples bracket the onset of thrust displacement on the Oritsume Fault between ~5.8 and 4.9 Ma. Late Pleistocene to Holocene fluvial terraces mapped along the Maibechi River (near section line A-A′; Figure 3a) have been warped across the hinge of the hanging wall fault-related fold (Chinzei, 1966), indicating that reverse-sense slip and fault-related folding is ongoing today.

4.1.2. Noheji Fault

We also identifed growth strata in the forelimb of the fault-related fold at two locations along the Noheji Fault. At site NH-1 (Figure 5a), steeply dipping (strike and dip of 350°, 46°E) Pliocene rocks of the Togawa Formation in the forelimb of the anticline near the southern tip of the fault are unconformably overlain by a gently east dipping (dip of ~10°E) cobble conglomerate and sandstone. At site NH-2 (Figure 5a) near the southern tip of the Noheji Fault, gently dipping marine terrace gravels and sands of the Takamoriyama Formation (Kudo, 2005) unconformably overlie steeply dipping strata of the Togawa Formation in the forelimb of the fold. We interpret this unconformity and the decrease in dip up section to mark the transition from pregrowth to growth strata associated with the initiation of thrust displacement on the Noheji Fault.

The timing of contraction along this structure was determined from new tephrachronology at two sites (Figure 5a). At site NH-1, two U-Pb zircon ages from tephras interbedded with sediments from steeply dipping pregrowth beds below the unconformity yielded ages of 2.24 (+0.08, −0.06) and 2.2 (+0.03, −0.07) Ma (Figure 5b). These agree with published zircon fission track ages for the pregrowth Togawa Formation of 3.6 and 2.6 Ma from a correlative section (Kudo, 2005) and represent a maximum estimate for the initiation of contraction along the Noheji Fault. The age of gently dipping beds atop the unconformity at these two sites place a minimum bound on the timing of thrust initiation. At site NH-1, new U-Pb zircon ages from the gently dipping growth beds above the unconformity constrain the deposit to 0.32 (+0.11, −0.04) Ma (Figure 5b). At site NH-2 the unconformity is overlain by gently dipping beds of the Takamoriyama Formation that contain an interbedded tephra recognized as the 0.33–0.22 Ma Bo-P tephra (Machida et al., 1985; Miyauchi, 1988). This combination of age data at these two sites brackets the onset of thrust displacement on the Noheji Fault to between ~2.2 Ma and 0.3 Ma, contemporary with slip along the Oritsume Fault, which began contractional deformation ~5 Ma.

4.2. Miocene Extension

Miocene extension along fore-arc faults is recorded by growth strata in the hanging wall of each fault system that record lateral thickness variations and syntectonic depositional facies. Extensional growth strata associated with fore-arc faults have the following characteristics (Figure 2): (1) The total thickness of synextensional strata is greater in the hanging wall than in the footwall. (2) The thickness of synextensional strata increases toward the basin bounding normal fault, (3) synextensional strata in the hanging wall may be in normal fault contact with basement in the footwall, (4) sediments at the base of the extensional growth sequence may contain clasts derived from local basement rocks exposed in the hanging wall of the fault, and (5) synextensional strata record a relatively rapid deepening of depositional facies, and postextensional strata record slow subsidence and basin filling.

4.2.1. Oritsume Fault

Stratigraphic and structural data indicate the Oritsume Fault formed by inversion of an inherited extensional fault that accommodated west-side down, displacement during the Miocene. This interpretation is supported by three lines of evidence. First, Miocene sediment is thicker in the hanging wall of the Oritsume Fault than in the footwall. The hanging wall sedimentary section is 1,250 to 2,100 m thick and includes complete sections of the Shiratorigawa and Sannohe groups (Figure 4). The sedimentary section exposed in the footwall, in contrast, is only 400–500 m thick and is missing the Yotsuyaku and Keiseitoge Formations from the Shiratorigawa Group and the Shitazaki and Kubo Formations of the Sannohe Group (Figure 4). Therefore, approximately 750 to 1,700 m of sedimentary section present in the hanging wall is absent in the footwall (Figure 4). This ~1 km difference in sediment thickness over a horizontal distance of $<$10 km requires the presence of a structural high in the footwall and creation of accommodation space west of the Oritsume Fault. With Plio-Quaternary contractional displacement along the Oritsume Fault restored, the elevation of the basement cover contact restores to a position ~400–1,000 m lower in the hanging wall than in the footwall.

Second, basal Miocene strata in the hanging wall of the Oritsume Fault have lithologies and geometries consistent with extensional growth strata. Basal strata of the Yotsuyaku Formation, which exists only in the hanging wall of the Oritsume Fault (Figures 3a and 4), are basement-bearing boulder to cobble alluvial conglomerates (Yagishita et al., 2006; Yagishita & Komori, 2000). These units are in normal fault contact with basement rocks (Figure 3a, site OT-2) (Yagishita et al., 2006) and contain paleo-flow indicators that suggest transport away from the fault, toward the west-northwest (Yagishita et al., 2006; Yagishita & Komori, 2000). The total thickness of the Yotsuyaku and Keiseitoge Formations is 150–300 m near the Oritsume Fault but thins westward and pinches out to zero thickness approximately 8 km west of the fault (Yagishita & Komori, 2000). These observations are consistent with deposition in the hanging wall of a normal fault during Miocene time.

Third, subsidence recorded within hanging wall sediments is consistent with deposition in an extensional basin. The Yotsuyaku Formation records rapid subsidence, with lignite-bearing terrestrial sediments at the base of the section and shallow marine siliciclastics interbedded with the volcaniclastic Keiseitoge Formation (Figure 4) (Yagishita & Komori, 2000). An increase in paleo-water depth up-section within the Yotsuyaku and Keiseitoge Formations (Figure 4) is consistent with a deepening of an extensional basin during continued fault slip. At the top of the section, the cessation of extension is recorded in overlying units, which show no or slow subsidence, and is present in both the hanging wall and footwall (Figure 4). The Kadonosawa, Suenomatsuyama, Shitazaki, and Kubo Formations do not show a clear increase in thickness toward the Oritsume Fault and are present in both the hanging wall and the footwall (e.g., Chinzei, 1966). Sedimentary facies in the Kadonosawa and Suenomatsuyama Formations record a gradual increase of paleo-water depth from littoral to deep marine, and the total thickness of these units in the footwall is 200–500 m less than that in the hanging wall (Figure 4). The overlying Shitazaki and Kubo Formations do not show clear thickness variations with respect to the Oritsume Fault. We interpret the Kadonosawa through the Kubo Formations to have been deposited during the last stages of fault-related extension or immediately following the cessation of extension in a basin where the rate of sedimentation occasionally outpaced the rate of generation of accommodation space.

Our interpretation of synextensional growth strata in the Yotsuyaku Formation and postextensional subsidence during the deposition of the Keiseitoge through Kubo Formations (Figure 4) brackets the duration of extensional slip on the Oritsume Fault. The initiation of extension is indicated by the age of the basal Yotsuyaku Formation. Existing zircon fission track and K-Ar ages in the Nisatai Dacite constrain the age of the base of the Yotsuyaku Formation to between ~23.9 ± 1.4 Ma and 21.0 ± 0.3 Ma (Hoshi & Matsubara, 1998; Tagami et al., 1995). We interpret the first postextensional growth strata to be within the base of Kadonosawa Formation, the oldest unit present in both the hanging wall and footwall of the Oritsume Fault. Published biostratigraphic data constrain the age of the Kadonosawa Formation to ~16–15 Ma (Irizuki & Matsubara, 1994; Yagishita & Komori, 2000) (Figure 4). We therefore consider that the timing of extensional deformation along the Oritsume Fault occurred from ~24–21 Ma until ~16–15 Ma.

4.2.2. Futaba Fault

Similar to the Oritsume Fault, multiple lines of evidence indicate that the Futaba Fault (Figure 7) experienced west-side down extensional displacement prior to the Pliocene. First, there is a thicker sequence of Neogene stratigraphy in the hanging wall of the Futaba Fault than in the footwall. The Neogene sedimentary section in

the hanging wall of the Futaba Fault, including the Shiramizu through Taga groups, has a total thickness of 1,800 to 2,200 m (Figure 8). In contrast, the sedimentary section in the footwall (cores A, A-1, N-1, and N-2; Figure 7) is only ~800 m thick (Figure 8). This footwall section is missing nearly the entire Miocene Yunagaya Group and the entirety of the Takaku and Shirado groups (Figure 8). Therefore, approximately 1,000–1,400 m of Miocene to Pliocene hanging wall sedimentary section is missing from the footwall. In addition, restoration of ~2–3 km of contractional deformation that has occurred since the Pliocene (Regalla et al., 2010) places the basement cover contact 600 to 1,100 m lower in the hanging wall than in the footwall. This difference of hanging wall and footwall sediment thickness is consistent with the creation of accommodation space in the hanging wall of an active extensional fault during the period of deposition of the Yunagaya, Takaku, and Shirado groups.

Second, Miocene extension is supported by variations in sedimentary facies and depositional environment in the Miocene Yunagaya Group, which records a progression from terrestrial to deep marine environments (e.g., Suto et al., 2005). The Kunugidaira Formation, at the base of the Yunagaya Group, is a Miocene fluvial deposit present in both the hanging and footwalls of the Futaba Fault (Suto et al., 2005). Up section, the deposits transition to the shallow marine deposits of the Goyasu Formation and the middle bathyal deposits (~500–1,000 m) of the Kamenoo and Mizunoya Formations (Suto et al., 2005). This facies succession is consistent with the interpretation that the Yunagaya Group is composed of synextensional strata deposited in the hanging wall of an active normal fault. In this interpretation, the Kunugidaira Formation is either a prerift unit or the earliest synrift sediments deposited during a period where the sediment supply exceeded the accommodation space created by extension, and the Goyasu, Kamenoo, and Mizunoya Formations were deposited in a fault-bound submarine basin where accommodation space created by fault slip exceeded sedimentation rate. The sediments overlying the Kamenoo Formation, near the top of the Yunagaya Group, record a shallowing of depositional environments, consistent with basin filling following the cessation of extension.

Third, analysis of the geomorphic evolution of channels developed in the hanging wall mountain range predicts a listric geometry for the Futaba Fault system (Regalla, Kirby, et al., 2013), supporting the interpretation that the fault reactivated an inherited structure that accommodated Miocene extension. This interpretation is further bolstered by thrust inversion of an extensional system identified along the Nagamachi-Rifu Fault (Kato et al., 2006; Sato et al., 2004), which projects into the northern tip of the Futaba Fault. It is likely that the two faults sole into a common detachment at depth.

Ages at the base and top of the section of Miocene sediments present in the hanging wall but absent in the footwall of the Futaba Fault bracket the duration of extensional faulting. Zircon fission track ages from the tuff member of the Kunugidaira Formation, the oldest unit present in only the hanging wall of the fault, yield ages of 20.8 ± 1.2 Ma (Figure 8) (Suto et al., 2005) and provide an estimate of the timing of initiation of extensional slip. The cessation of extension occurred prior to or during the deposition of the upper Takaku Group, the youngest sediments present in only the hanging wall of the Futaba Fault. Published biostratigraphic correlations and fission track ages within the Takaku Group bracket the termination of extensional deformation to ~16 and 15.9 ± 0.7 Ma (Figure 8) (Suto et al., 2005). Given the limited exposure of hanging wall strata, it is not possible to quantify lateral thickness variations in hanging wall deposits with distance from the Futaba Fault that help distinguish synextensional from postextensional deposits. It is possible therefore that a portion of the deposition of the Miocene Takaku and Shirado groups postdated extension and that the cessation of extension occurred prior to 16 Ma.

4.3. Kinematic Modeling and Fault Geometry

We used trishear kinematic modeling to quantify subsurface fault geometry for the Oritsume, Noheji, and Futaba Faults and to reproduce their Neogene slip histories. These fault geometries were then used in forward models that simulated extension and contractional inversion to test if observed bed dips and stratigraphic thicknesses are consistent with Plio-Quaternary thrust inversion of Miocene extensional structures, to place bounds on the total magnitudes of thrust and normal displacement, and to evaluate the geometry and mechanics of faults susceptible to slip inversion. The results of the models here reproduce only the dip-slip component of deformation in a 2D cross section and cannot constrain the potential effects of deformation related to lateral slip out of the plane of section. However, existing geologic data suggest lateral motion, if present, is a minor component of deformation within these fault systems. Below we discuss the fault geometries determined for the Oritsume, Noheji, and Futaba Faults but limit our discussion of

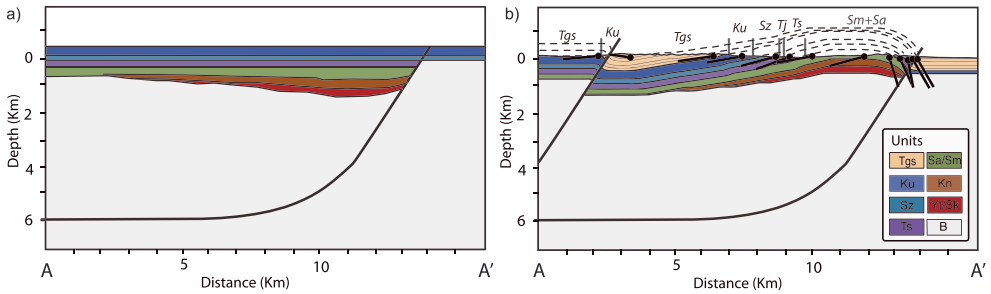

Figure 9. Cross sections across the Oritsume Fault along section line A-A′. See Figure 3 for location. (a) Section after 700 m of extensional slip and deposition of the Shiratorigawa and lower Sannohe groups, during the late Miocene. (b) Section after 1,900 m of contractional inversion, present day.

extension and thrust inversion to the Oritsume and Futaba Faults, as extensional growth strata were not identified along the Noheji Fault.

4.3.1. Oritsume Fault

Trishear models of thrust slip along the Oritsume Fault and fault-related fold simulate bed dips along profile line A-A′ (Figure 3). The initial geometry of trishear models included basement overlain by 1,200 m of subhorizontal sediment of the Suenomatsuyama through Togawa Formations. The fault-related anticline in the hanging wall of the Oritsume Fault in 2D Move is best reproduced if the fault has a nonplanar, listric geometry. Trishear models with a planar, west dipping fault cannot reproduce the west dipping beds observed in the hanging wall of the Oritsume Fault. Instead, a fault with a listric geometry is required to generate both the hanging wall anticline and the west dipping beds in the back-limb of the fold, and this listric geometry was similarly adopted during inverse trishear modeling. Results of forward trishear models indicate that bed dips at the surface are best replicated by 1.8–2.0 km of slip on a fault with a ramp angle of 55°-65° that soles to a subhorizontal detachment at 6–7 km depth (Table 1). Similarly, results of inverse trishear models indicate that the fault-related fold is best restored given 1.4–2.0 km of slip along a 46°–57° fault ramp (Table 1). Detachment depth is difficult to constrain with inverse models, and a range of detachments depths are allowable. However, inverse models with detachment depths of 6–7.5 km, comparable to that obtained from forward modeling, are able to replicate observed bed dips, contacts, and fault tip position observed in the field. Differences in fault geometry between forward and inverse model results are a function of differences in how the two models assign the curvature of listric faults, the relative importance of bed dip versus contact position in assessing model fit, and the range of parameter variability allowed in each approach. The listric fault geometry obtained from kinematic modeling is consistent with the interpretation that the Oritsume Fault is the result of contractional inversion of an extensional half-graben.

The best fit fault geometry determined from modeling of the fault-related fold was then used as the input fault geometry for extensional models. Models of extension along the Oritsume Fault assumed initially gently west dipping basement-cover contact. Sediment added during and following extension replicated the observed thickness of the synextensional Yotsuyaku Formation and postextensional Kadonosawa through Kubo Formations (Figure 4). Inversion of the best fit extensional model was then performed using a range of best fit model parameters determined from contractional models (Table 1). Extensional models with 400–750 m of normal displacement on a fault with a listric shape best reproduce the observed eastward increase in stratigraphic thickness in the synextensional Yotsuyaku, Keiseitoge, and Kadonosawa Formations in the hanging wall (Figure 9a). Models of thrust inversion with 1,800–2,000 m of thrust displacement best reproduce the geometry of the contractional fault-related fold and the observed locations of stratigraphic contacts (Figure 9b).

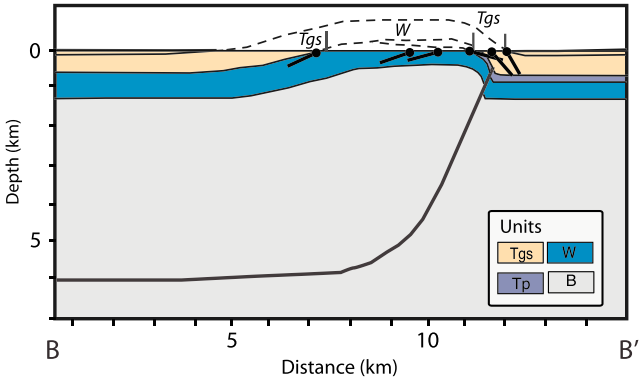

Figure 10. Cross section across the Noheji Fault along line B-B′. See Figure 5 for location. Section depicts the Noheji Fault and fault-related fold after ~475 m of contraction, present day.

4.3.2. Noheji Fault

The Noheji Fault is located ~10 km west of the Oritsume Fault, within the hanging wall block of this structure. Given that the Oritsume Fault has a listric geometry, the two systems likely merge at depth at a

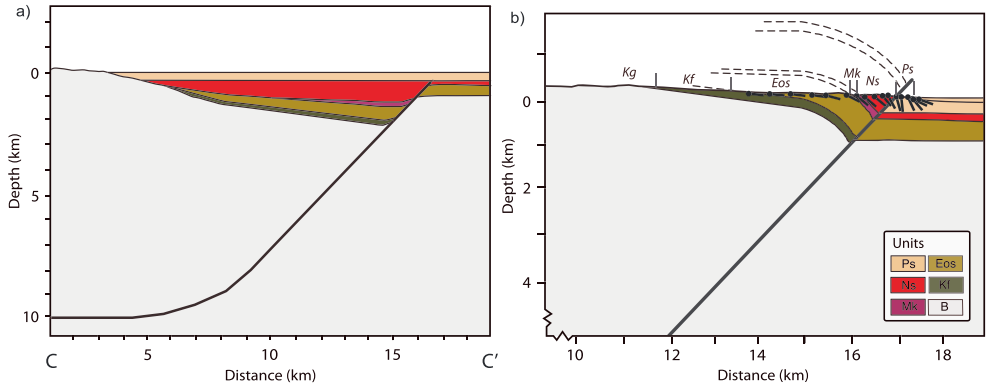

Figure 11. Cross sections across the Futaba Fault, along line C-C′. See Figure 7 for location. (a) Section after 1,000 m of extensional slip and deposition of the Miocene and Pliocene sedimentary section, during the late Miocene. (b) Section after 2,100 m of contractional inversion, present day.

common detachment level. We therefore model the Noheji Fault with a listric geometry and a detachment at 6–7 km depth in both forward and inverse models. Forward contractional models of the Noheji Fault simulate the hanging wall anticline along profile B-B′ (Figure 5a). The initial model geometry consisted of basement overlain by 1,300 m of initially planar strata of the Miocene to Pliocene Wadagawa through Togawa Formations. The spatial extent and thickness of the basal Miocene volcanic rocks are poorly constrained, and therefore, this unit was modeled as part of basement. No synextensional strata associated with the Noheji Fault are exposed at the surface; we therefore only model contractional deformation for this structure.

The contractional fault-related fold at the southern tip of the Noheji Fault is best reproduced by forward models in 2D Move given 860–1,100 m of dip displacement along a fault with a 55°–65° ramp that flattens to a detachment at 6 km depth (Figure 10 and Table 1). This fault geometry is consistent with the best fit fault detachment depth on the adjacent Oritsume Fault and reproduces the fault-related fold geometry along section B-B′ (Figure 5a). Inverse models that restore the fault-related fold developed in Pliocene units similarly reproduce fault geometries with a 46°–64° ramp that flattens to subhorizontal at 6–7 km depths (Table 1).

4.3.3. Futaba Fault

The geometry of the Futaba Fault in the shallow subsurface (<5–10 km) is reasonably well known from both previous forward kinematic models (Regalla et al., 2010) and new inverse kinematic models of the hanging wall anticline at the southern tip of the fault. Fault-related fold geometry is best reproduced in forward kinematic models given 2–3 km of thrust displacement along a 40°–55° west dipping thrust fault (Regalla et al., 2010).

These results are consistent with new, inverse trishear kinematic models that indicate bedding in the fault-related fold restore with 2.1–2.7 km of slip along a 39° to 58° ramp (Table 1). The robustness of these solutions is demonstrated by the independently reached agreement between the inverse and forward models. Due to the lack of backlimb structural data for the associated anticline, only the planar fault ramp was modeled. Previous work on the geomorphology and incision rates of fluvial systems in the hanging wall of the Futaba Fault, however, places some bounds on the fault geometry at depth (Regalla, Kirby, et al., 2013). Both the position of slope-break knickzones and the spatial distribution of basin-averaged erosion rates across these geomorphic features are best reproduced if streams evolve in the hanging wall of a listric fault whose dip changes from 40°–55° to subhorizontal at 10–15 km depth (Regalla, Kirby, et al., 2013). This fault geometry is similar to the geometry determined from seismic reflection surveys of the Nagamachi-Rifu Fault at the northern end of the Futaba Fault system (Kato et al., 2006; Sato et al., 2002) and is consistent with thrust inversion of an inherited listric normal fault.

We integrate these constraints on the timing, geometry, and kinematics of shortening along the Futaba Fault with trishear models to quantify the magnitude of extension and contractional inversion. Initial state models of the Futaba Fault include basement overlain by gently seaward dipping sediments of the Cretaceous through Eocene Futaba and Shiramizu groups. Extensional slip on the Futaba Fault was modeled with a listric fault geometry with a 40°–55° ramp that flattens to a detachment at 10 km depth. The variations in thickness between the footwall and hanging wall Miocene stratigraphic sections constrain the magnitude of

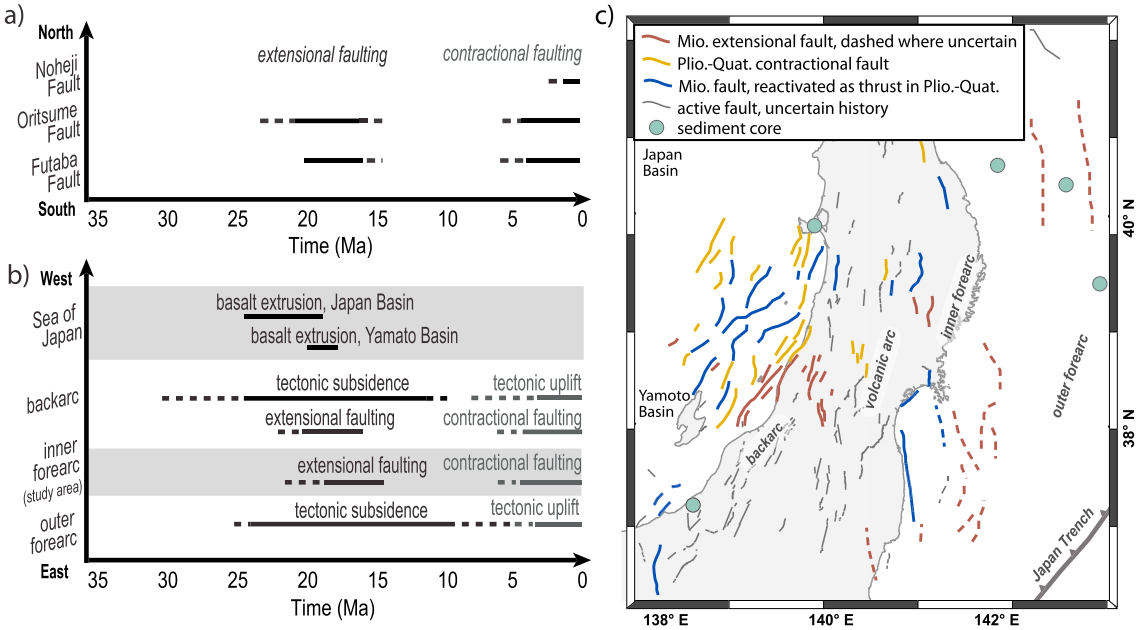

Figure 12. (a) Summary of timing of slip along the inner fore-arc Noheji, Oritsume, and Futaba Faults as determined in this study. The dashed lines indicate uncertainty in timing. Note that the duration of extension and contraction along all three faults is synchronous. (b) Summary of the timing of tectonic events in northern Honshu, Japan. Miocene extension, extrusion of seafloor basalts, and tectonic subsidence occur at the same time in the back arc and fore arc. Similarly, Plio-Quaternary contraction and tectonic uplift occur synchronously in the back arc and fore arc. (c) Map showing the distribution of faults with known extension, contraction, and inversion histories, and the locations of sediment cores used to determine back-arc and fore-arc subsidence histories. Timing and kinematics in Figures 12b and 12c after Tamaki and Kobayashi (1988), Jolivet and Tamaki (1992), Ingle (1992), Okamura et al. (1995), Takano (2002), Sato et al. (2002), Okamura (2003), Sato et al. (2004), Nakajima (2006), Okada and Ikeda (2012), and Regalla, Kirby, et al. (2013).

extensional displacement in extensional models. Best fit models require 1,000–1,500 m of extensional displacement along a 40°–55° west dipping fault (Figure 11a). This magnitude of displacement and fault geometry allows for the deposition of an ~1,000 m thick sedimentary sequence filling the hanging wall basin. This thickness is consistent with the 1,000–1,400 m of missing Miocene section in the footwall of the Futaba Fault. The postextensional system was subject to contractional inversion, given best fit previously published model parameters for Plio-Quaternary contraction (Table 1) (Regalla et al., 2010). Models of contractional inversion successfully reproduced the observed fault-related fold geometry (Figure 11b) given 2–3 km of thrust displacement.

5. Discussion

5.1. Neogene Tectonic Inversion in the Northeast Japan Fore Arc

Our results provide new evidence for Plio-Quaternary thrust inversion of listric, Miocene extensional faults in the fore arc of Northeast Japan, indicating that thrust inversion has occurred >50 km east of the modern volcanic arc. We identify and date growth strata that bracket the initiation of thrust displacement along these structures to 5.8–4.9 Ma along the Oritsume Fault and <2.2 Ma along the Noheji Fault (Figure 12a). Contraction along these faults is synchronous with the 5.6–3.6 Ma initiation of thrust slip on the Futaba Fault (Regalla et al., 2010) and with deformation along a network of Plio-Quaternary thrust faults and fault-related folds present along the eastern margin of the Sea of Japan (Okada & Ikeda, 2012; Okamura, 2003), across the volcanic arc (Nakajima, 2006) and offshore in the outer fore arc (Boston et al., 2017) (Figure 12). Our data also reveal an earlier phase of extensional deformation along the Oritsume and Futaba Faults between ~24–20 Ma and ~16–15 Ma (Figure 12a), based on the presence of synextensional strata in the hanging walls of these faults. Extension along the Futaba and Oritsume faults was synchronous with Miocene extension along the Nagamachi-Rifu Fault near Sendai (Kato et al., 2006; Sato et al., 2002), along offshore listric faults east of Sendai (Kato et al., 1996), and with extensional faulting documented across the back arc (Nakajima, 2006; Okada & Ikeda, 2012) (Figure 12). Kinematic modeling of fault-related fold geometries indicates that these structures are best replicated by ~0.5 to ~1.5 km of

extension, followed by ~1–2.5 km of thrust slip along 40°–65° west dipping, listric faults with subhorizontal detachments at 6 to 10 km depth (Table 1). These fault geometries are consistent with Plio-Quaternary thrust inversion of Miocene extensional half graben and provide a spatiotemporal link between faulting in the inner fore arc and Neogene tectonic subsidence/uplift patterns in the back arc and outer fore arc.

Miocene extensional faulting in the inner fore arc along the Oritsume and Futaba Faults during the opening of the Sea of Japan was associated with crustal thinning, rift-related tectonic subsidence, and approximately trench orthogonal $\sigma_{h\text{-min}}$ directions (Ingle, 1992; Sato, 1994). Extension related to the opening of the Sea of Japan was also associated with widespread tectonic subsidence in the back arc between ~25 Ma and ~15 Ma (Ingle, 1992) and in the outer fore arc from ~25 to 5 Ma (Arthur et al., 1980; von Huene et al., 1982; Regalla, Fisher, et al., 2013) (Figure 12). This period of tectonic subsidence was coeval with the rapid deepening of the sediment-water interface recorded in the hanging wall of the Oritsume and Futaba Faults from ~26 to 16 Ma (Figures 4, 8, and 12). Fore-arc extension was part of an eastward migration of back-arc extension that stepped from the Japan and Yamato basins at ~24–18 Ma, to the eastern margin of the Sea of Japan at ~21 to ~18 Ma, and to the back arc and arc of Honshu at ~18 to ~13 Ma (Jolivet & Tamaki, 1992; Kaneoka et al., 1990; Nakajima, 2006; Okamura et al., 1995; Regalla, Fisher, et al., 2013), during which time extension occurred along the Oritsume and Futaba Faults (Figure 12). The total magnitude of Miocene extension decreases from the back arc to the fore arc, with the inner fore-arc Oritsume and Futaba Faults accommodating only ~10% of the magnitude of extension observed in the back arc and extensional faults in the outer fore arc accommodating only ~10% of that within the inner fore arc. These observations suggest that although the total magnitude of extensional deformation decreases from back arc to fore arc, the fore arc still experienced permanent deformation related to the opening of the Sea of Japan.

Starting between ~8 and 5 Ma, the arc transitioned to a compressive stress state with a trench orthogonal $\sigma_{h\text{-max}}$ (e.g., Sato & Amano, 1991). This transition initiated contraction across a network of faults in the upper plate, many of which evolved as inverted extensional structures (Okada & Ikeda, 2012; Okamura, 2003; Okamura et al., 1995; Sato & Amano, 1991). At the same time, the arc experienced a regional transition to tectonic uplift, documented in both fore-arc and back-arc subsidence records (Ingle, 1992; Regalla, Fisher, et al., 2013), shallowing of sedimentary facies in near coastal basins (Ingle, 1992; Kato et al., 1996; Sato, 1986; Sato, 1994) and flights of uplifted marine terraces that span $>$500 km of the Tohoku coastline (Koike & Machida, 2001; Suzuki, 1989). This period of regional uplift and shallowing of sedimentary facies coincides with the ~6 to 4 Ma onset of contractional faulting along the Oritsume, Noheji, and Futaba Faults in the inner fore arc. These inner fore-arc faults accommodate 90–55% less shortening than faults in the back arc (cf., Okada & Ikeda, 2012). However, while the shortening along inverted back-arc faults recovers, on average, less than half of the magnitude of Miocene extension, shortening along inverted fore-arc faults can exceed extension by 200–300%. The correlation between the reorientation of stress state, contraction along trench parallel faults, and the magnitude of crustal uplift across the entire arc throughout the Pliocene through Holocene indicates that net permanent strain in the inner fore arc has been dominated by shortening of the fore arc and associated rock uplift.

The temporal correlation between fault kinematics and subsidence across the northern Japan arc during the Neogene suggests that the changes in inner fore-arc deformation documented here along the Oritsume, Noheji, and Futaba Faults are part of a margin-wide reorganization of deformation driven by lithospheric scale processes and changes in plate boundary tractions operating over millions of years. Previous work has often decoupled the mechanisms responsible for this deformation into those affecting the upper plate fault kinematics and those affecting outer fore-arc subsidence. Neogene changes in fault kinematics in the overriding plate have been attributed to variations in the absolute velocities of the upper and lower plates (e.g., Heuret et al., 2007; Heuret & Lallemand, 2005; Lallemand et al., 2005, 2008) or changes in far-field kinematic boundary conditions (Jolivet et al., 1994; Jolivet & Tamaki, 1992; Sato, 1994), while tectonic subsidence documented in the outer fore arc has been independently attributed to basal tectonic erosion from the Miocene to the present (e.g., von Huene et al., 1982; von Huene & Lallemand, 1990). However, the correlation of both extension and subsidence in the Miocene, and later between contraction and uplift in the Plio-Quaternary, across a 500–1,000 km wide region in the upper plate of the Japan subduction zone suggests that the state of stress and vertical motions of both the fore arc and back arc may be the collective response to dynamic changes in slab geometry (Regalla, Fisher, et al., 2013), as may result from accelerations in convergence rate (Buiter et al., 2001; Capitanio et al., 2009; Furlong et al., 1982; Regalla, Fisher, et al., 2013) or from

foundering of the subducted slab through the mantle transition zone (e.g., Capitanio et al., 2010; Fukao et al., 2001; Goes et al., 2008). Such changes in slab geometry have the potential to produce periodic variations in upper plate stress that affect the vertical tectonics and stress state of the entire fore-arc-arc-back-arc system and can precondition the upper plate with network of faults whose geometries and mechanics are favorable for reactivation and inversion during later deformation events.

5.2. Implications for Present-Day Fore-Arc Strain Accumulation in Northeast Japan

Although the net, permanent deformation of the overriding plate throughout the Pliocene and Quaternary has been dominated by E-W directed shortening, numerous recent earthquakes in the fore arc of Japan following the 2011 Tohoku earthquake exhibit surface displacements and normal faulting focal mechanisms consistent with E-W extension (Hasegawa et al., 2012; Hirose et al., 2011; Imanishi et al., 2012; Kato et al., 2011; Okada et al., 2011). These events have been proposed to reflect responses to static stress changes due to elastic or viscoelastic deformation in the upper plate following the 2011 Tohoku-oki megathrust earthquake (Kato et al., 2011; Miyazawa, 2011; Okada et al., 2011; Sun et al., 2014; Toda, Lin, & Stein, 2011; Toda, Stein, & Lin, 2011; Wang et al., 2012). Of particular note is the west-side-down extensional surface displacement documented along the Idosawa and Yunodake Faults, which bound the southeastern Abukuma massif south of the Futaba Fault (Imanishi et al., 2012; Kato et al., 2011; Kobayashi et al., 2012). Similarities in the geomorphic expression of the hanging walls of the Idosawa and Futaba Faults, and the presence of east vergent fault-related folds developed in Pliocene strata associated with both faults, suggest that the Idosawa-Yunodake-Futaba Fault network has accommodated net west-side up contractional displacement, uplifting the Abukuma Mountains over the past ~5–3 Ma (Regalla et al., 2010; Regalla, Kirby, et al. 2013). This is opposite to the sense of slip that occurred during the Idosawa *M*7.0 earthquake in 2011 and implies that that normal-slip displacement during this event represents an inversion of the long-term, Plio-Quaternary, thrust slip sense.

Similar transient inversions of fault kinematics have been observed in the fore arc of Chile, where the most recent paleoseismic event on a normal fault system has thrust sense displacement (Loveless et al., 2010), and on faults in the Eastern California Shear zone, where left-lateral slip occurred on structures with net right-lateral offset, following the 1999 Hector mine earthquake (Fialko et al., 2002). In regions like subduction fore arcs that experience cyclic changes to stress loading, inversion of the long-term slip sense may be possible on faults that are anomalously weak due to low frictional coefficient, large damage zones associated with reactivated structures, or the presence of fluids (e.g., Fialko et al., 2002; Hampel & Hetzel, 2008; Loveless et al., 2010). Such conditions may be met in the present day on fore-arc faults in Japan, which have experienced at least two phases of tectonic activity, which may be associated with zones of high fluid pressure (Okada et al., 2010; Sato, 1994; Sibson, 2009; Tong et al., 2012), and which experience significant stress changes following megathrust events (Okada et al., 2011; Toda, Lin, & Stein, 2011; Toda, Stein, & Lin, 2011; Yoshida et al., 2015). Modeling of Coulomb stress changes in the upper plate induced by the megathrust earthquake cycle suggests that both reverse and extensional slips can be promoted along fore-arc faults, depending on the location of the fault relative to the megathrust slip patch (e.g., Farías et al., 2011; Loveless et al., 2010). Reactivated fore-arc faults, like the Futaba, Oritsume, and Noheji Faults in Japan, may therefore be examples of structures that could host seismicity following megathrust event, and the slip induced by static stress changes or viscoelastic transients need not have the same kinematics as net geologic displacements.

We use best fit fault geometries from kinematic modeling to estimate the range of parameters that would allow faults in the fore arc of Northeast Japan to experience thrust inversion of extensional faults, assuming 2-D Mohr Coulomb failure where $\tau_c = c + \mu(\sigma_n - P_f)$. Fault dips of 40°–65° are within an optimal range for thrust inversion for $\mu = 0.1$ to 0.4 (e.g., Sibson, 1985), and static friction (μ) values of 0.2 to 0.4, although small, are reasonable for fault fabrics developed in muscovite schists, talc schists, and montmorillonite bearing systems (Ikari et al., 2011), such as are present in the Mesozoic basement of Northeast Japan (e.g., Isozaki, 1997; Saito & Hashimoto, 1982). Faults with 40°–65° dips can be reactivated without generating new faults in the upper plate, assuming that new faults have coefficients of internal friction $\geq$0.4 and cohesion $\geq$0 MPa for differential stresses of 10 to 100 MPa or greater, and fluid pressures between hydrostatic and lithostatic. These parameters require fault shear strengths of 10 to >75 MPa. These values are consistent with previous estimates of differential stress between <25 and 180 MPa (Seno, 1999; Yang et al., 2013; Yoshida et al., 2015), and fault shear strengths of 40–90 MPa (Yang et al., 2013) for the Northeast Japan fore arc.

In addition, an overpressured midcrust has been suggested based on the presence of bright reflectors, low-velocity zones, anomalous V_p/V_s ratios, and high electrical conductivity beneath northern Honshu arc and fore arc (e.g., Okada et al., 2010; Sibson, 2009; Tong et al., 2012). The high-angle, listric, fore-arc faults we document are therefore geometrically and mechanically suitable for thrust inversion of inherited normal faults during the Plio-Quaternary.

Faults with dips of 40°–65° and μ of 0.2 to 0.4, such as the ramps of the Oritsume, Noheji, and Futaba Faults, are also susceptible to normal sense displacements given the changes in orientation and magnitude of the stress field that can occur following large-magnitude megathrust earthquakes. Normal slip can occur along these faults if the megathrust event is associated with a large, nearly complete stress drop where σ_1 can rotate toward vertical, as has been suggested from focal mechanism inversions of outer fore-arc aftershocks following the 2011 Tohoku-oki earthquake and from borehole breakouts at Integrated Ocean Drilling Program Site C0019, which crosses the plate boundary (Hasegawa et al., 2012; Lin et al., 2013; Yoshida et al., 2015). Normal sense slip can occur on faults with dips of 40°–65° and $\mu = 0.2$ to 0.4, for differential stress <25 MPa in cases of no fluid overpressure, and can occur at differential stresses less than 10 MPa if pore fluid pressures approach 70% to 90% of lithostatic. Slip on subhorizontal fault detachments with dips of 10°–30° and $\mu = 0.2$ to 0.4 at depths of 6–10 km is favored only for cases of very high fluid pressures greater than 90% to 95% of lithostatic. These parameters are consistent with inferences of high fluid pressures and low differential stress in the upper plate following the megathrust earthquake (e.g., Hasegawa et al., 2011; Tong et al., 2012; Yang et al., 2013). These data suggest that the Oritsume, Noheji, and Futaba Faults are geometrically and mechanically favorable to experience changes in slip sense between thrust and normal and can fail in response to changes in plate boundary tractions over both geologic (~10^6 years) and seismic (~10^2–10^3 years) timescales.

These observations highlight the dynamic nature of fore-arc faults and their sensitivity to changes in the upper plate stress field imparted both by long-term, geologic forcings, and by short-term variations in plate coupling during the megathrust seismic cycle. We suggest that the repeated history of deformation and fault inversion during the Neogene has primed the fore arc of Northeast Japan with a network of weak faults that allow the fore arc to deform in response to changes in plate boundary tractions over both decadal and millennial time scales. These data suggest that upper plate earthquakes triggered by megathrust events need not have the same kinematics as the long-term geologic slip sense. The potential for such temporal variability in slip sense has important implications for assessing the seismic hazard posed by fore-arc faults, and their potential to fail in response to changes in the stress field during the seismic cycle (cf., Aron et al., 2013; Farías et al., 2011; Imanishi et al., 2012; Morell et al., 2017; Sherrod & Gomberg, 2014). The kinematic history of inner fore-arc faults therefore serves as an important record of past plate boundary dynamics that provides insight into the conditions under which seismogenic failure occurs along faults in the upper plate of subduction systems.

6. Conclusions

New structural and geochronologic data illuminate the timing and kinematics of slip inversion contraction along three fault systems within the inner fore arc of the Northeast Japan margin. Our results reveal that Miocene extension occurred along the Oritsume and Futaba Faults from ~24–21.0 Ma until ~16–15 Ma. New U-Pb zircon ages from tephras interbedded with contractional growth strata along the Oritsume and Noheji Faults bracket the onset of reverse slip to between ~6 to 4 Ma for the Oritsume Fault and to <2.2 Ma for the Noheji Fault. Kinematic fault-related fold modeling indicates that inner fore-arc deformation reflects Plio-Quaternary inversion of Miocene listric extensional faults, with ramps that dip 40–65° west and that sole into a subhorizontal detachment at 6–10 km depth. These data suggest that the onset of inner fore-arc normal faulting was associated with upper plate extension and subsidence related to the opening of the Sea of Japan and that the transition to Plio-Quaternary contraction was synchronous with contraction and uplift across the back arc and fore arc. We suggest that variations in the orientation of the maximum compressive stress caused by the dynamic subduction processes that lead to the initiation and cessation of upper plate extension during the Neogene primed the fore arc with a network of weak faults susceptible to subsequent slip inversion. The geometries of the Oritsume, Noheji, and Futaba Faults are capable of hosting contractional slip related to the arc-normal compressive stress state that has dominated the Plio-Quaternary and can also host normal slip in response to transient changes in the orientation and

magnitude of fore-arc stress following large megathrust events, such as the 2011 Tohoku-oki earthquake. These data reinforce the notion that the permanent strain history along fore-arc faults is a key factor in understanding the sensitivity of fore-arc deformation to variations in boundary conditions at the plate interface over both geologic and seismogenic time scales.

Acknowledgments
Funding was provided by a grant from the National Science Foundation Tectonics Program grant EAR-0809939 to D.M.F. and E.K., Geologic Society of America Graduate Research Grants, and the P.D. Krynine Memorial Fund. The authors thank Gaku Kimura, Kyoko Tonegawa, Hiroko Watanabe, Jun Kameda, and Asuka Yamaguchi for scientific and logistical support, and Kristin Morell for comments on early versions of the manuscript. We also thank Yuzuru Yamamoto and Kohtaro Ujiie for their detailed reviews and suggestions for improvement to the manuscript. The authors acknowledge the use of the Move Software Suite granted by Midland Valley's Academic Software Initiative. Geologic, structural, stratigraphic, and chronologic data used herein are accessible in manuscript figures, and in the citations therein. Input geologic data for trishear kinematic modeling can be accessed in Table 1 and in the supporting information.

References

Allmann, B. P., & Shearer, P. M. (2009). Global variations of stress drop for moderate to large earthquakes. *Journal of Geophysical Research*, *114*, B01310. https://doi.org/10.1029/2008JB005821

Allmendinger, R. W. (1998). Inverse and forward numerical modeling of trishear fault-propagation folds. *Tectonics*, *17*(4), 640–656. https://doi.org/10.1029/98TC01907

Allmendinger, R. W., & González, G. (2010). Invited review paper: Neogene to Quaternary tectonics of the coastal Cordillera, northern Chile. *Tectonophysics*, *495*(1-2), 93–110. https://doi.org/10.1016/j.tecto.2009.04.019

Aoyagi, K., & Omokawa, M. (1993). Diagenesis of Neogene diatoms and their importance as a source of petroleum in Japan. *Island Arc*, *2*(4), 273–279. https://doi.org/10.1111/j.1440-1738.1993.tb00093.x

Aron, F., Allmendinger, R. W., Cembrano, J., González, G., & Yáñez, G. (2013). Permanent fore-arc extension and seismic segmentation: Insights from the 2010 Maule earthquake, Chile. *Journal of Geophysical Research: Solid Earth*, *118*, 724–739. https://doi.org/10.1029/2012JB009339

Arthur, M. A., von Huene, R., & Adelseck, C. G. (1980). Sedimentary evolution of the Japan fore-arc region off northern Honshu, Legs 56 and 57, Deep Sea Drilling Project in *Scientific Party, Initial Reports of the Deep Sea Drilling Project, Legs 56 and 57 (Part 1)* (pp. 521–612). Washington DC: U.S. Government Printing Office.

Audin, L., Lacan, P., Tavera, H., & Bondoux, F. (2008). Upper plate deformation and seismic barrier in front of Nazca subduction zone: The Chololo Fault System and active tectonics along the Coastal Cordillera, southern Peru. *Tectonophysics*, *459*(1-4), 174–185. https://doi.org/10.1016/j.tecto.2007.11.070

Balfour, N., Cassidy, J., Dosso, S., & Mazzotti, S. (2011). Mapping crustal stress and strain in southwest British Columbia. *Journal of Geophysical Research: Solid Earth*, *116*, B03314. https://doi.org/10.1029/2010JB008003

Bangs, N. L. N., Gulick, S. P. S., & Shipley, T. H. (2006). Seamount subduction erosion in the Nankai Trough and its potential impact on the seismogenic zone. *Geology*, *34*(8), 701–704. https://doi.org/10.1130/G22451.1

Boston, B., Moore, G. F., Nakamura, Y., & Kodaira, S. (2017). Forearc slope deformation above the Japan Trench megathrust: Implications for subduction erosion. *Earth and Planetary Science Letters*, *462*, 26–34. https://doi.org/10.1016/j.epsl.2017.01.005

Buchanan, P. G., & McClay, K. R. (1991). Sandbox experiments of inverted listric and planar fault systems. *Tectonophysics*, *188*(1-2), 97–115. https://doi.org/10.1016/0040-1951(91)90317-L

Buiter, S. J. H., Govers, R., & Wortel, M. J. R. (2001). A modelling study of vertical surface displacements at convergent plate margins. *Geophysical Journal International*, *147*(2), 415–427. https://doi.org/10.1046/j.1365-246X.2001.00545.x

Capitanio, F. A., Morra, G., & Goes, S. (2009). Dynamics of plate bending at the trench and slab-plate coupling. *Geochemistry, Geophysics, Geosystems*, *10*, Q04002. https://doi.org/10.1029/2008GC002348

Capitanio, F. A., Stegman, D. R., Moresi, L. N., & Sharples, W. (2010). Upper plate controls on deep subduction, trench migrations and deformations at convergent margins. *Tectonophysics*, *483*(1-2), 80–92. https://doi.org/10.1016/j.tecto.2009.08.020

Cardozo, N., & Brandenburg, J. P. (2014). Kinematic modeling of folding above listric propagating thrusts. *Journal of Structural Geology*, *60*, 1–12. https://doi.org/10.1016/j.jsg.2013.12.004

Chinzei, K. (1966). Younger Tertiary geology of the Mabechi River Valley, northeast Honshu, Japan. *Journal of Faculty of Science, Univeristy of Tokyo, Section II*, *16*, 161–208.

Erslev, E. (1991). Trishear fault-propogation folding. *Geology*, *19*(6), 617–620. https://doi.org/10.1130/0091-7613(1991)019%3C0617:TFPF%3E2.3.CO;2

Farías, M., Comte, D., Roecker, S., Carrizo, D., & Pardo, M. (2011). Crustal extensional faulting triggered by the 2010 Chilean earthquake: The Pichilemu seismic sequence. *Tectonics*, *30*, TC6010. https://doi.org/10.1029/2011TC002888

Fialko, Y., Sandwell, D., Agnew, D., Simons, M., Shearer, P., & Minster, B. (2002). Deformation on nearby faults induced by the 1999 Hector Mine earthquake. *Science*, *297*(5588), 1858–1862. https://doi.org/10.1126/science.1074671

Fisher, D., & Byrne, T. (1987). Structural evolution of underthrusted sediments, Kodiak Islands, Alaska. *Tectonics*, *6*(6), 775–793. https://doi.org/10.1029/TC006i006p00775

Fisher, D. M., Gardner, T. W., Marshall, J. S., Sak, P. B., & Protti, M. (1998). Effect of subducting seafloor roughness on fore-arc kinematics, Pacific coast, Costa Rica. *Geology*, *26*(5), 467–470. https://doi.org/10.1130/0091-7613(1998)026%3C0467:EOSSFR%3E2.3.CO;2

Fukao, Y., Widiyantoro, S., & Obayashi, M. (2001). Stagnant slabs in the upper and lower mantle transition region. *Reviews of Geophysics*, *39*(3), 291–323. https://doi.org/10.1029/1999RG000068

Fulton, P., Brodsky, E. E., Kano, Y., Mori, J., Chester, F., Ishikawa, T., … Toczko, S. (2013). Low coseismic friction on the Tohoku-Oki fault determined from temperature measurements. *Science*, *342*(6163), 1214–1217. https://doi.org/10.1126/science.1243641

Furlong, K. P., Chapman, D. S., & Alfeld, P. W. (1982). Thermal modeling of the geometry of subduction with implication for the tectonics of the overriding plate. *Journal of Geophysical Research*, *87*(B3), 1786–1802. https://doi.org/10.1029/JB087iB03p01786

Gardner, T., Marshall, J., Merritts, D., Bee, B., Burgette, R., Burton, E., … Fisher, D. (2001). Holocene forearc block rotation in response to seamount subduction, southeastern Peninsula de Nicoya, Costa Rica. *Geology*, *29*(2), 151–154. https://doi.org/10.1130/0091-7613(2001)029%3C0151:HFBRIR%3E2.0.CO;2

Geological Survey of Japan (2003). Geological map of Japan, 1:1,00,000, (3rd ed.,), 2nd CD-ROM version. Digital Geoscience Map Series G-1. Geological Survey of Japan, AIST.

Goes, S., Capitanio, F. A., & Morra, G. (2008). Evidence of lower-mantle slab penetration phases in plate motions. *Nature*, *451*(7181), 981–984. https://doi.org/10.1038/nature06691

Hampel, A. (2002). Migration history of the Nazca Ridge along the Peruvian active margin: A re-evaluation. *Earth and Planetary Science Letters*, *203*(2), 665–679. https://doi.org/10.1016/S0012-821X(02)00859-2

Hampel, A., & Hetzel, R. (2008). Slip reversals on active normal faults related to the inflation and deflation of magma chambers: Numerical modeling with application to the Yellowstone-Teton region. *Geophysical Research Letters*, *35*, L07301. https://doi.org/10.1029/2008GL033226

Hasegawa, A., Yoshida, K., Asano, Y., Okada, T., Iinuma, T., & Ito, Y. (2012). Change in stress field after the 2011 great Tohoku-Oki earthquake. *Earth and Planetary Science Letters*, *355-356*, 231–243. https://doi.org/10.1016/j.epsl.2012.08.042

Hasegawa, A., Yoshida, K., & Okada, T. (2011). Nearly complete stress drop in the 2011 M_w 9.0 off the Pacific coast of Tohoku earthquake. *Earth, Planets and Space*, *63*(7), 703–707. https://doi.org/10.5047/eps.2011.06.007

Hassani, R., Jongmans, D., & Chéry, J. (1997). Study of plate deformation and stress in subduction processes using two-dimensional numerical models. *Journal of Geophysical Research*, *102*(B8), 17,951–17,965. https://doi.org/10.1029/97JB01354

Heuret, A., Funiciello, F., Faccenna, C., & Lallemand, S. (2007). Plate kinematics, slab shape and back-arc stress: A comparison between laboratory models and current subduction zones. *Earth and Planetary Science Letters*, *256*(3-4), 473–483. https://doi.org/10.1016/j.epsl.2007.02.004

Heuret, A., & Lallemand, S. (2005). Plate motions, slab dynamics and back-arc deformation. *Physics of the Earth and Planetary Interiors*, *149*(1-2), 31–51. https://doi.org/10.1016/j.pepi.2004.08.022

Hiroi, Y., Kishi, S., Nohara, T., Sato, K., & Goto, J. (1998). Cretaceous high-temperature rapid loading and unloading in the Abukuma metamorphic terrane, Japan. *Journal of Metamorphic Geology*, *16*(1), 67–81. https://doi.org/10.1111/j.1525-1314.1998.00065.x

Hirose, F., Miyaoka, K., Hayashimoto, N., Yamazaki, T., & Nakamura, M. (2011). Outline of the 2011 off the Pacific coast of Tohoku earthquake (M_w 9.0)—Seismicity: foreshocks, mainshock, aftershocks, and induced activity—. *Earth, Planets and Space*, *63*(7), 513–518. https://doi.org/10.5047/eps.2011.05.019

Hoshi, H., & Matsubara, M. (1998). Early Miocene paleomagnetic results from the Ninohe area, NE Japan: Implications for arc rotation and intra-arc differential rotations. *Earth, Planets and Space*, *50*, 22–33.

Ikari, M. J., Marone, C., & Saffer, D. M. (2011). On the relation between fault strength and frictional stability. *Geology*, *39*(1), 83–86. https://doi.org/10.1130/G31416.1

Ikeda, Y., Imaizumi, T., Togo, M., Hirakawa, K., Miyauchi, T., & Sato, H. (2002). *Atlas of Active Faults in Japan*. Tokyo, Japan: University of Tokyo Press.

Imanishi, K., Ando, R., & Kuwahara, Y. (2012). Unusual shallow normal-faulting earthquake sequence in compressional northeast Japan activated after the 2011 off the Pacific coast of Tohoku earthquake. *Geophysical Research Letters*, *39*, L09306. https://doi.org/10.1029/2012GL051491

Ingle, J. (1992). Subsidence of the Japan Sea: Stratigraphic evidence from ODP sites and onshore sections. *Proceeding of the Ocean Drilling Program, Scientific Results*, *127/128*(2), 1197–1218.

Irizuki, T., & Matsubara, M. (1994). Vertical changes of depositional environments of the lower to middle Miocene Kadonosawa Formation based on analysis of fossil ostracode faunas. *Journal of the Geological Society of Japan*, *100*(2), 136–149_2. https://doi.org/10.5575/geosoc.100.136

Ishizuka, O., & Uto, K. (1995). K-Ar ages from the Neogene volcanic rocks in the Ninohe District, Iwate Prefecture. *Annual Meeting of the Society of Volcanology of Japan*, *4*, 207–211.

Isozaki, Y. (1997). Jurassic accretion tectonics of Japan. *Island Arc*, *6*(1), 25–51. https://doi.org/10.1111/j.1440-1738.1997.tb00039.x

Isozaki, Y., Maruyama, S., & Furuoka, F. (1990). Accreted oceanic materials in Japan. *Tectonophysics*, *181*(1-4), 179–205. https://doi.org/10.1016/0040-1951(90)90016-2

Iwata, N., Tanaka, H., & Kato, Y. (2000). Ar^{40}-Ar^{39} and K-Ar mineral ages of the Tabito composite mass in the southern Abukuma Mountains, northeast Japan. *Journal of Mineralogy Petrology and Economic Geology*, *95*(1), 1–11. https://doi.org/10.2465/ganko.95.1

Jolivet, L., & Tamaki, K. (1992). Neogene kinematics in the Japan Sea region and volcanic activity of the Northeast Japan arc. *Proceeding of the Ocean Drilling Program, Scientific Results*, *127/128*(2), 1311–1331.

Jolivet, L., Tamaki, K., & Fournier, M. (1994). Japan Sea, opening history and mechanism: A synthesis. *Journal of Geophysical Research*, *99*(B11), 22,237–22,259. https://doi.org/10.1029/93JB03463

Kamada, K., Hata, M., Kubo, K., & Sakamoto, T. (1990). Geologic map of Hachinohe, 1:200,000 sheet, *Geological Survey of Japan*, copyright 1991.

Kaneoka, I., Notsu, K., Takigami, Y., Fujioka, K., & Sakai, H. (1990). Constraints on the evolution of the Japan Sea based on 40Ar-39Ar ages and Sr isotopic ratios for volcanic rocks of the Yamato Seamount chain in the Japan Sea. *Earth and Planetary Science Letters*, *97*(1-2), 211–225. https://doi.org/10.1016/0012-821X(90)90109-B

Kato, A., Sakai, S., & Obara, K. (2011). A normal-faulting seismic sequence triggered by the 2011 off the Pacific coast of Tohoku earthquake: Wholesale stress regime changes in the upper plate. *Earth, Planets and Space*, *63*(7), 745–748. https://doi.org/10.5047/eps.2011.06.014

Kato, N., Sato, H., & Umino, N. (2006). Fault reactivation and active tectonics on the fore-arc side of the back-arc rift system, NE Japan. *Journal of Structural Geology*, *28*(11), 2011–2022. https://doi.org/10.1016/j.jsg.2006.08.004

Kato, S., Akiba, F., & Moriya, S. (1996). The Upper Cretaceous-Cenozoic stratigraphy and geologic structure in the offshore Soma area, northeast Japan. *Journal of Geological Society of Japan*, *102*(12), 1039–1051. https://doi.org/10.5575/geosoc.102.1039

Kimura, G. (1994). The latest Cretaceous-early Paleogene rapid growth of accretionary complex and exhumation of high pressure series metamorphic rocks in northwestern Pacific margin. *Journal of Geophysical Research*, *99*(B11), 22,147–22,164. https://doi.org/10.1029/94JB00959

Kington, J., & Tobin, H. (2011). Balanced cross sections, shortening estimates, and the magnitude of out-of-sequence thrusting in the Nankai Trough accretionary prism, Japan. Paper presented at AGU Fall Meeting Abstracts.

Kobayashi, T., Tobita, M., Koarai, M., Okatani, T., Suzuki, A., Noguchi, Y., … Miyahara, B. (2012). InSAR-derived crustal deformation and fault models of normal faulting earthquake (M_j 7.0) in the Fukushima-Hamadori area. *Earth, Planets and Space*, *64*(12), 1209–1221. https://doi.org/10.5047/eps.2012.08.015

Koike, K., & Machida, H. (2001). *Atlas of Quaternary marine terraces in the Japanese Islands*. Tokyo: University of Tokyo Press.

Kubo, K., Yanigisawa, Y., Toshimitsu, S., Banno, Y., Kaneko, N., Yoshioka, T., & Takagi, T. (2002). Geology of the Kawamae and Ide District. *Geological Survey of Japan Quadrangle Series, 1:50,000*, *7*(58–59), 1–136.

Kubo, K., Yanigisawa, Y., Yamamoto, T., Komazawa, M., Hiroshima, T., & Sudo, S. (2003). Geological map of Japan 1:200,000 Fukushima, Geological Survey of Japan.

Kudo, T. (2005). Geologic map of Towada, 1:50,000 sheet, Geological Survey of Japan, AIST, copyright 2005.

Kylander-Clark, A. R. C., Hacker, B. R., & Cottle, J. M. (2013). Laser-ablation split-stream ICP petrochronology. *Chemical Geology*, *345*, 99–112. https://doi.org/10.1016/j.chemgeo.2013.02.019

Lallemand, S., Heuret, A., & Boutelier, D. (2005). On the relationships between slab dip, back-arc stress, upper plate absolute motion, and crustal nature in subduction zones. *Geochemistry, Geophysics, Geosystems*, *6*, Q09006. https://doi.org/10.1029/2005GC000917

Lallemand, S., Heuret, A., Faccenna, C., & Funiciello, F. (2008). Subduction dynamics as revealed by trench migration. *Tectonics*, *27*, TC3014. https://doi.org/10.1029/2007TC002212

Lin, W., Conin, M., Moore, J. C., Chester, F. M., Nakamura, Y., Mori, J. J., … Eguchi, N. (2013). Stress state in the largest displacement area of the 2011 Tohoku-Oki earthquake. *Science*, *339*(6120), 687–690. https://doi.org/10.1126/science.1229379

Loveless, J. P., Allmendinger, R. W., Pritchard, M. E., & González, G. (2010). Normal and reverse faulting driven by the subduction zone earthquake cycle in the northern Chilean fore arc. *Tectonics*, *29*, TC2001. https://doi.org/10.1029/2009TC002465

Ludwig, K. R., & Mundil, R. (2002). Extracting reliable U-Pb ages and errors from complex populations of zircons from Phanerozoic tuffs. *Geochimica et Cosmochimica Acta*, *66*(15A), 463.

Machida, H., Arai, F., & Momose, M. (1985). Aso-4 ash: A widespread tephra and its implications to the events of late Pleistocene in and around Japan. *Bulletin of the Volcanological Society of Japan 2nd Series*, *30*, 49–70.

Mitra, S., & Islam, Q. T. (1994). Experimental (clay) models of inversion structures. *Tectonophysics*, *230*(3-4), 211–222. https://doi.org/10.1016/0040-1951(94)90136-8

Mitsui, S. (1971). Studies on the mechanism and deformation of sedimentary rocks in the Iwaki area of the Jaban coal-field, Fukushima Prefecture. *Science Reports of the Tohoku University, 2nd series*, *42*(3), 199–272.

Miyauchi, T. (1988). Late Pleistocene marine terrace correlation and chronology in the northern Northeast Japan, *The Institute of The Kuroshio Sphere*, *Kochi University*.

Miyazawa, M. (2011). Propagation of an earthquake triggering front from the 2011 Tohoku-Oki earthquake. *Geophysical Research Letters*, *38*, L23307. https://doi.org/10.1029/2011GL049795

Morell, K. D. (2016). Seamount, ridge, and transform subduction in southern Central America. *Tectonics*, *35*, 357–385. https://doi.org/10.1002/2015TC003950

Morell, K. D., Fisher, D. M., Gardner, T. W., La Femina, P., Davidson, D., & Teletzke, A. (2011). Quaternary outer fore-arc deformation and uplift inboard of the Panama Triple Junction, Burica Peninsula. *Journal of Geophysical Research*, *116*, B05402. https://doi.org/10.1029/2010JB007979

Morell, K. D., Regalla, C., Leonard, L. J., Amos, C., & Levson, V. (2017). Quaternary rupture of a crustal fault beneath Victoria, British Columbia, Canada. *GSA Today*, *27*(3), 4–10. https://doi.org/10.1130/GSATG291A.1

Nakajima, T. (2006). Uplift of the Ou Backbone Range in Northeast Japan at around 10 Ma and its implication for the tectonic evolution of the eastern margin of Asia. *Palaeogeography, Palaeoclimatology, Palaeoecology*, *241*(1), 28–48. https://doi.org/10.1016/j.palaeo.2006.06.009

National Institute of Advanced Industrial Science and Technology (2012). Online active fault database of Japan, Tsukuba, Japan. Retrieved from: http://riodb02.ibase.aist.go.jp/activefault/index_e.html

Niitsuma, N. (2004). Japan Trench and tectonics of the Japanese island arcs. *The Island Arc*, *13*(1), 306–317. https://doi.org/10.1111/j.1440-1738.2003.00427.x

Oakley, D. O., & Fisher, D. M. (2015). Inverse trishear modeling of bedding dip data using Markov chain Monte Carlo methods. *Journal of Structural Geology*, *80*, 157–172. https://doi.org/10.1016/j.jsg.2015.09.005

Okada, S., & Ikeda, Y. (2012). Quantifying crustal extension and shortening in the back-arc region of Northeast Japan. *Journal of Geophysical Research*, *117*, B01404. https://doi.org/10.1029/2011JB008355

Okada, T., Umino, N., & Hasegawa, A. (2010). Deep structure of the Ou mountain range strain concentration zone and the focal area of the 2008 Iwate-Miyagi Nairiku earthquake, NE Japan—Seismogenesis related with magma and crustal fluid. *Earth, Planets and Space*, *62*(3), 347–352. https://doi.org/10.5047/eps.2009.11.005

Okada, T., Yoshida, K., Ueki, S., Nakajima, J., Uchida, N., Matsuzawa, T., … Hasegawa, A. (2011). Shallow inland earthquakes in NE Japan possibly triggered by the 2011 off the Pacific coast of Tohoku earthquake. *Earth, Planets and Space*, *63*(7), 749–754. https://doi.org/10.5047/eps.2011.06.027

Okamura, Y. (2003). Fault-related folds and an imbricate thrust system on the northwestern margin of the northern Fossa Magna region, central Japan. *The Island Arc*, *12*(1), 61–73. https://doi.org/10.1046/j.1440-1738.2003.00379.x

Okamura, Y., Watanabe, M., Morijiri, R., & Satoh, M. (1995). Rifting and basin inversion in the eastern margin of the Japan Sea. *Island Arc*, *4*(3), 166–181. https://doi.org/10.1111/j.1440-1738.1995.tb00141.x

Ozawa, A., & Mimura, K. (1993). Geologic map of Aomori, 1:200,000 sheet, *Geological Survey of Japant*, copyright 1993.

Regalla, C., Fisher, D., & Kirby, E. (2010). Timing and magnitude of shortening within the inner fore arc of the Japan Trench. *Journal of Geophysical Research*, *115*, B03411. https://doi.org/10.1029/2009JB006603

Regalla, C., Fisher, D. M., Kirby, E., & Furlong, K. P. (2013). Relationship between outer forearc subsidence and plate boundary kinematics along the Northeast Japan convergent margin. *Geochemistry, Geophysics, Geosystems*, *14*, 5227–5243. https://doi.org/10.1002/2013GC005008

Regalla, C., Kirby, E., Fisher, D., & Bierman, P. (2013). Active forearc shortening in Tohoku, Japan: Constraints on fault geometry from erosion rates and fluvial longitudinal profiles. *Geomorphology*, *195*, 84–98. https://doi.org/10.1016/j.geomorph.2013.04.029

Regard, V., Lagnous, R., Espurt, N., Darrozes, J., Baby, P., Roddaz, M., … Hermoza, W. (2009). Geomorphic evidence for recent uplift of the Fitzcarrald Arch (Peru): A response to the Nazca Ridge subduction. *Geomorphology*, *107*(3-4), 107–117. https://doi.org/10.1016/j.geomorph.2008.12.003

Royden, L. H., & Husson, L. (2006). Trench motion, slab geometry and viscous stresses in subduction systems. *Geophysical Journal International*, *167*(2), 881–905. https://doi.org/10.1111/j.1365-246X.2006.03079.x

Ryder, I., Rietbrock, A., Kelson, K., Bürgmann, R., Floyd, M., Socquet, A., … Carrizo, D. (2012). Large extensional aftershocks in the continental forearc triggered by the 2010 Maule earthquake, Chile. *Geophysical Journal International*, *188*(3), 879–890. https://doi.org/10.1111/j.1365-246X.2011.05321.x

Saffer, D. M., & Tobin, H. J. (2011). Hydrogeology and mechanics of subduction zone forearcs: Fluid flow and pore pressure. *Annual Review of Earth and Planetary Sciences*, *39*(1), 157–186. https://doi.org/10.1146/annurev-earth-040610-133408

Saito, Y., & Hashimoto, M. (1982). South Kitakami region: An allochthonous terrane in Japan. *Journal of Geophysical Research*, *87*(B5), 3691–3696. https://doi.org/10.1029/JB087iB05p03691

Sato, H. (1986). Geologic development of the Cenozoic system in central northeast Honshu (between Sakata and Furukawa), Japan (Part 1). *Science Reports Tohoku University 2nd Sereis (Geology)*, *88*, 1–32.

Sato, H. (1994). The relationship between late Cenozoic tectonic events and stress field and basin development in northeast Japan. *Journal of Geophysical Research*, *99*(B11), 22,261–22,274. https://doi.org/10.1029/94JB00854

Sato, H., & Amano, K. (1991). Relationship between tectonics, volcanism, sedimentation and basin development, late Cenozoic, central part of northern Honshu, Japan. *Sedimentary Geology*, *74*(1-4), 323–343. https://doi.org/10.1016/0037-0738(91)90071-K

Sato, H., Imaizumi, T., Yoshida, T., Ito, H., & Hasegawa, A. (2002). Tectonic evolution and deep to shallow geometry of Nagamachi-Rifu active fault system NE Japan. *Earth, Planets and Space*, *54*(11), 1039–1043. https://doi.org/10.1186/BF03353298

Sato, H., Yoshida, H., Iwasaki, T., Sato, T., Ikeda, Y., & Umino, N. (2004). Late Cenozoic tectonic development of the back arc region of central northern Honshu, Japan, revealed by recent deep seismic profiling. *Journal of the Japanese Association for Petroleum Technology*, *69*(2), 145–154. https://doi.org/10.3720/japt.69.145

Seno, T. (1999). Syntheses of the regional stress fields of the Japanese islands. *Island Arc*, *8*(1), 66–79. https://doi.org/10.1046/j.1440-1738.1999.00225.x

Seno, T., Stein, S., & Gripp, A. (1993). A model for the motion of the Philippine Sea plate consistent with NUVEL-1 and geological data. *Journal of Geophysical Research*, *98*(B10), 17,941–17,948. https://doi.org/10.1029/93JB00782

Sherrod, B., & Gomberg, J. (2014). Crustal earthquake triggering by pre-historic great earthquakes on subduction zone thrusts. *Journal of Geophysical Research: Solid Earth*, *119*, 1273–1294. https://doi.org/10.1002/2013JB010635

Sibson, R. H. (1985). A note on fault reactivation. *Journal of Structural Geology*, *7*(6), 751–754. https://doi.org/10.1016/0191-8141(85)90150-6

Sibson, R. H. (2009). Rupturing in overpressured crust during compressional inversion—The case from NE Honshu, Japan. *Tectonophysics*, *473*(3-4), 404–416. https://doi.org/10.1016/j.tecto.2009.03.016

Sun, T., Wang, K., Iinuma, T., Hino, R., He, J., Fujimoto, H., … Ohta, Y. (2014). Prevalence of viscoelastic relaxation after the 2011 Tohoku-oki earthquake. *Nature*, *514*(7520), 84–87. https://doi.org/10.1038/nature13778

Suto, I., Yanagisawa, Y., & Ogasawara, K. (2005). Tertiary geology and chronostratigraphy of the Joban area and its environs, northeastern Japan. *Geological Survey Research Report*, *56*(11–12), 375–409.

Suzuki, T. (1989). Late Quaternary crustal movements deduced from marine terraces and active faults, Japan Coastal region, Northeast Japan. *Geographical Reports of Tokyo Metropolotan University*, *24*, 31–42.

Tagami, T., Uto, K., Matsuda, T., Hasebe, N., & Matsumoto, A. (1995). K-Ar biotite and fission-track zircon ages of the Nisatai Dacite, Iwate Prefecture, Japan: A candidate for tertiary age standard. *Geochemical Journal*, *29*(3), 207–211. https://doi.org/10.2343/geochemj.29.207

Takano, O. (2002). Changes in depositional systems and sequences in response to basin evolution in a rifted and inverted basin: An example from the Neogene Niigata-Shin'etsu basin, Northern Fossa Magna, central Japan. *Sedimentary Geology*, *152*(1-2), 79–97. https://doi.org/10.1016/S0037-0738(01)00286-X

Tamaki, K., & Kobayashi, K. (1988). Geomagneitc anamoly lineations in the Sea of Japan. *Marine Sciences Monthly*, *20*, 705–710.

Tobin, H. J., & Saffer, D. M. (2009). Elevated fluid pressure and extreme mechanical weakness of a plate boundary thrust, Nankai Trough subduction zone. *Geology*, *37*(8), 679–682. https://doi.org/10.1130/G25752A.1

Toda, S., Lin, J., & Stein, R. S. (2011). Using the 2011 M_w 9.0 off the Pacific coast of Tohoku earthquake to test the Coulomb stress triggering hypothesis and to calculate faults brought closer to failure. *Earth, Planets and Space*, *63*(7), 725–730. https://doi.org/10.5047/eps.2011.05.010

Toda, S., Stein, R. S., & Lin, J. (2011). Widespread seismicity excitation throughout central Japan following the 2011 M=9.0 Tohoku earthquake and its interpretation by Coulomb stress transfer. *Geophysical Research Letters*, *38*, L00G03. https://doi.org/10.1029/2011GL047834

Tong, P., Zhao, D., & Yang, D. (2012). Tomography of the 2011 Iwaki earthquake (M 7.0) and Fukushima nuclear power plant area. *Solid Earth*, *3*(1), 43–51. https://doi.org/10.5194/se-3-43-2012

Tsushima, K. (1962). Geologic map of Noheji, 1:200,000 sheet, Geological Survey of Japan.

Ujiie, K., & Kimura, G. (2014). Earthquake faulting in subduction zones: Insights from fault rocks in accretionary prisms. *Progress in Earth and Planetary Science*, *1*(1), 7. https://doi.org/10.1186/2197-4284-1-7

van der Werff, W. (2000). Backarc deformation along the eastern Japan Sea margin, offshore northern Honshu. *Journal of Asian Earth Sciences*, *18*(1), 71–95. https://doi.org/10.1016/S1367-9120(99)00046-2

von Huene, R., & Lallemand, S. (1990). Tectonic erosion along the Japan and Peru convergent margins. *Geological Society of America Bulletin*, *102*(6), 704–720. https://doi.org/10.1130/0016-7606(1990)102%3C0704:TEATJA%3E2.3.CO;2

von Huene, R., Langeseth, M., Nasu, N., & Okada, H. (1982). A summary of Cenozoic tectonic history along the IPOD Japan Trench transect. *Geological Society of America Bulletin*, *93*(9), 829–846. https://doi.org/10.1130/0016-7606(1982)93%3C829:ASOCTH%3E2.0.CO;2

Wang, K., & Bilek, S. L. (2011). Do subducting seamounts generate or stop large earthquakes? *Geology*, *39*(9), 819–822. https://doi.org/10.1130/G31856.1

Wang, K., Hu, Y., & He, J. (2012). Deformation cycles of subduction earthquakes in a viscoelastic Earth. *Nature*, *484*(7394), 327–332. https://doi.org/10.1038/nature11032

Wang, K., Mulder, T., Rogers, G. C., & Hyndman, R. D. (1995). Case for very low coupling stress on the Cascadia Ssubduction Fault. *Journal of Geophysical Research*, *100*(B7), 12,907–12,918. https://doi.org/10.1029/95JB00516

Wesnousky, S. G., Scholz, C. H., Shimazaki, K., & Matsuda, T. (1984). Integration of geological and seismological data for the analysis of seismic hazard; a case study of Japan. *Bulletin of the Seismological Society of America*, *74*(2), 687–708.

Yagishita, K., Kawamorita, H., Horiai, D., Katsumasa, K., & Sasaki, M. (2006). A note on tectonic evolution within a Neogene basin: New evidence from the early to middle Miocene Ichinohe Basin, northeast Japan. *Geoscience Reports of Shizuoka University*, *33*, 1–7.

Yagishita, K., & Komori, K. (2000). Basin evolution within the Kitakami Massif, northeast Japan: Relationship between sedimentation, tectonics and volcanism in an incipient Neogene continental back-arc basin. *Sedimentary Geology*, *133*(1-2), 7–26. https://doi.org/10.1016/S0037-0738(00)00025-7

Yamaguchi, T. (1970). The Neogene of the northeastern part of the Shimokita Peninsula. Northeast Honshu, Japan—On the stratigraphic relation of the Tomari, the Gamanosawa and the "Sunagomata" Formations. *Journal of the Geological Society of Japan*, *76*(4), 185–197. https://doi.org/10.5575/geosoc.76.185

Yang, Y. R., Johnson, K. M., & Chuang, R. Y. (2013). Inversion for absolute deviatoric crustal stress using focal mechanisms and coseismic stress changes: The 2011 *M*9 Tohoku-oki, Japan, earthquake. *Journal of Geophysical Research: Solid Earth*, *118*, 5516–5529. https://doi.org/10.1002/jgrb.50389

Yoshida, K., Hasegawa, A., & Okada, T. (2015). Spatial variation of stress orientations in NE Japan revealed by dense seismic observations. *Tectonophysics*, *647-648*, 63–72. https://doi.org/10.1016/j.tecto.2015.02.013